Giant 10 (2022) 100096

Contents lists available at ScienceDirect

Giant

journal homepage: www.journals.elsevier.com/giant

Full-length article

Conformationally flexible dendronized cyclotetraveratrylenes (CTTV)s self-organize a large diversity of chiral columnar, Frank-Kasper and quasicrystal phases

Dipankar Sahoo, Mihai Peterca, Mohammad R. Imam, Benjamin E. Partridge, Qi Xiao, Virgil Percec *

Roy & Diana Vagelos Laboratories, Department of Chemistry, University of Pennsylvania, Philadelphia, PA 19104-6323, United States

ARTICLE INFO

Keywords:
Hierarchical
Self-organization
Self-assembly
Helical columns
Spherical helix
Frank-Kasper and quasicrystals

ABSTRACT

Primary structure endows the tertiary structure while the tertiary structure determines the function of hierarchical self-organizations. This is a well-established fundamental principle both for biological and non-biological synthetic assemblies. The role of the conformational flexibility-rigidity in this process is less understood. Here we select the conformationally flexible monodisperse tetramer of veratrole, 2,3,7,8,12,13,17,18-octamethoxy-5,10,15,20-tetrahydrotetrabenzo[a,d,g,j]-cyclododecatetraene, known as cyclotetraveratrylene (CTTV) and use it as an apex model to compare with the less flexible corresponding trimer known as cyclotriveratrylenes (CTV) and with the rigid triphenylene (Tp) and 1,3,5-trihydroxybenzene (THB) when dendronized with libraries of self-assembling dendrons and with n-alkyl groups. Unexpectedly, a large diversity of chiral helical assemblies including supramolecular columns assembled from chiral spheres and crowns, 12-fold quasi liquid crystals (QLC), Frank-Kasper A15 (space group $Pm\bar{3}n$) but not σ phases (space group $P4_2/mnm$), and supramolecular orientational memory effect (SOM) were observed in the case of the dendronized CTTV. The more rigid structures at the apex provide thermally more stable helical chiral periodic and quasiperiodic self-organizations with lowed dynamics which may facilitate the freezing of metastable rather than equilibrium structures. Conformational flexibility also changes the structure of the self-organization generated from supramolecular spheres. These experiments indicate that additional studies on the topic of conformational flexibility are desirable.

Introduction

Self-assembling dendrons, dendrimers and covalent and supramolecular dendronized polymers [1–56] self-organize a large diversity of chiral structures regardless of whether they are hierarchically assembled from chiral or achiral building blocks. Helical chirality and deracemization of a racemic helix [57–61] in crystal state are two of the most fundamental principles that mediate this process both in biological and in synthetic systems. The primary structure of the self-assembling dendrons and dendrimers including their generation number, multiplicity of their branching point, the dynamics and the flexibility of the supramolecular and covalent polymers and oligomers building their apex are key constructs of these helical assemblies. Libraries of self-assembling dendrons and dendrimers with different primary structure but identical apex functionality have been employed to construct a Periodic Table [29] of self-assembling dendrons correlating their primary structure to their tertiary structure. Different functional groups at the apex have been used to assemble supramolecular dendronized polymers *via* different H-bonding functional groups, donor-acceptor interactions, ionic-interactions including their solvation by crown-ethers and oligooxyethylenes [42,47,49–51,56,65] and their correlation has been compared with that of specific covalent polymers. Less is known about the role of the precise degrees of polymerization of covalent dendronized polymers on hierarchical self-organization although living polymerizations have been used [62–67] to correlate the degree of polymerization with tertiary structure. Living polymerizations provide only an average estimate of the degree of polymerization and its correlation to tertiary structure is limited by the very small molar fraction of chains with precise degree of polymerization [68–72]. Triphenylene (Tp) [34] represent a planar trimer of 1,2-dihydroxy benzene while CTV [33] and CTTV [73] represent perfectly monodisperse crown trimers and more conformationally flexible tetramers of veratrole. Therefore, a

* Corresponding author.
E-mail address: percec@sas.upenn.edu (V. Percec).

https://doi.org/10.1016/j.giant.2022.100096
Received 25 February 2022; Received in revised form 28 February 2022; Accepted 3 March 2022
Available online 4 March 2022

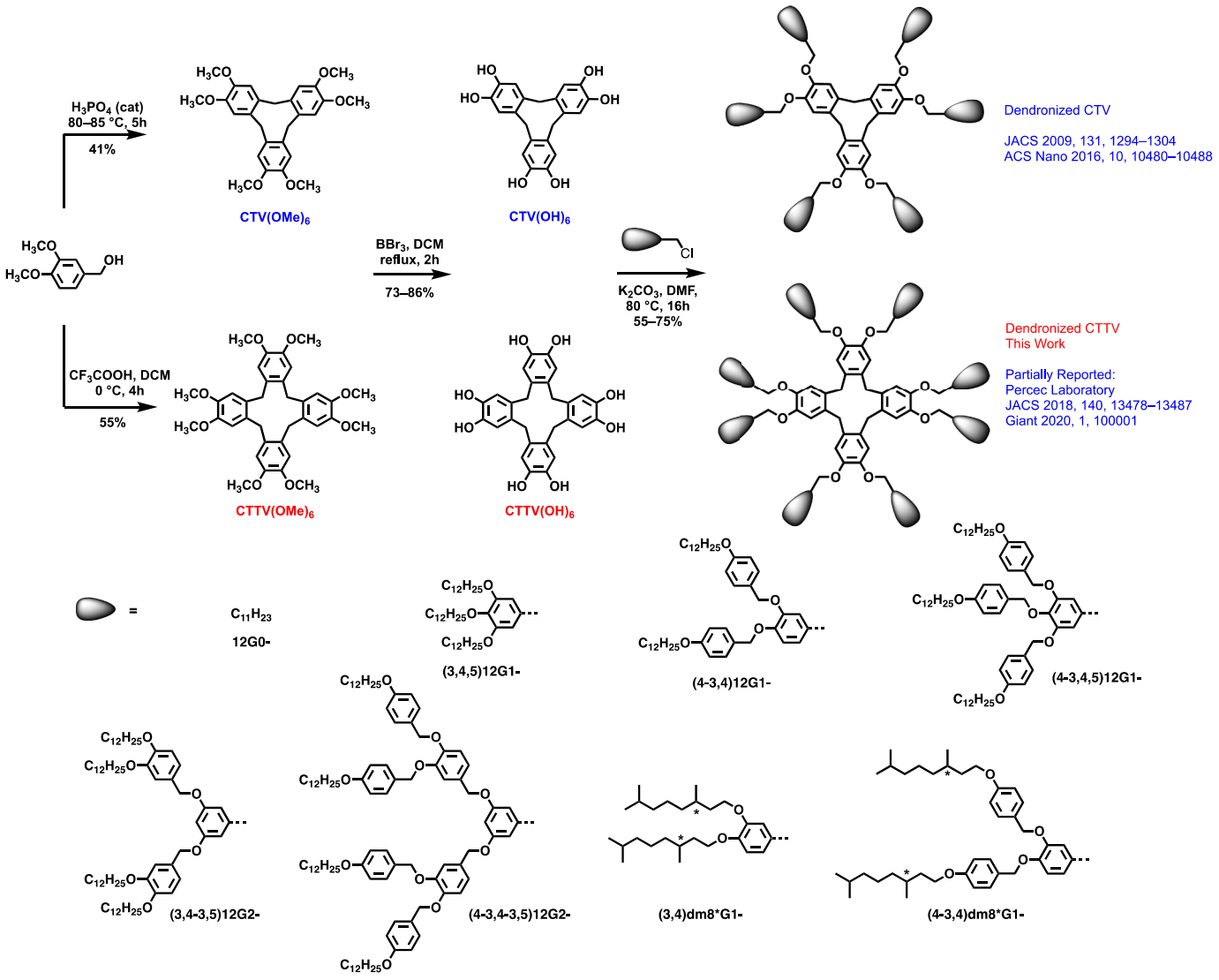

Fig. 1. Synthesis of dendronized CTV and CTTV.

comparison of the conformationally flexible dendronized CTTV with that of the less flexible CTV and Tp would bring some light on the role of conformational flexibility of a dendronized covalent apex on the corresponding tertiary structure. This publication reports the synthesis of *n*-alkyl-substituted and dendronized CTTV, provides the structural analysis of the corresponding self-organizations and compares them with those resulted from the more rigid CTV, triphenylenes and other assemblies to demonstrate the role of the conformational flexibility on their hierarchical self-organization. Two previous discoveries with dendronized CTTV prompted this series of experiments. The first chiral helical columnar hexagonal periodic array self-organized from chiral supramolecular spheres [73] and one of the few supramolecular orientational memory effects (SOM) observed at the transition between columnar hexagonal and Frank-Kasper A15 phase [74–79] prompted the current series of investigations.

Methods

Synthesis

The synthesis of the molecules including 2,3,7,8,12,13,17,18-octamethoxy-5,10,15,20-tetrahydrotetrabenzo[a,d,g,j]-cyclododecatetraene, known as cyclotetraveratrylene (CTTV) [80,81], *n*-dodecyl-substituted CTTV **12G0-CTTV** [82], dendronized CTTV including **(3,4,5)12G1-CTTV, (4-3,4,5)12G1-CTTV, (4-3,4)12G1-CTTV, (3,4-3,5)12G2-CTTV, (4-3,4-3,5)12G2-CTTV, (3,4)dm8*G1-CTTV**, and **(4-3,4)dm8*G1-CTTV** was reported previously by Percec laboratory but with the exception of **(3,4)dm8*G1-CTTV** were not characterized [73]. All of them were resynthesized by similar methods with even higher purities than previously reported.

NMR. ^{1}H NMR (500 MHz) and ^{13}C NMR (126 MHz) spectra were recorded on a Bruker DRX 500 instrument at 300 K using the indicated solvent.

High-performance liquid chromatography (HPLC). The purity of all CTTV final compounds was determined by a combination of thin-layer chromatography (TLC) on silica gel coated aluminum plates (with F254 indicator; layer thickness, 200 μm; particle size, 2–25 μm; pore size 60 Å, SIGMA-Aldrich) and high pressure liquid chromatography (HPLC) using THF as mobile phase at 1 mL/min, on a Shimadzu LC-10AT high pressure liquid chromatograph equipped with a Perkin Elmer LC-100 oven (40 °C), containing two Perkin-Elmer PL gel columns of 5×10^2 and 1×10^4 Å, a Shimadzu SPD-10A UV detector ($\lambda = 254$ nm), a Shimadzu RID-10A RI-detector, and a PE Nelson Analytical 900 Series integrator data station.

Matrix-assisted laser desorption/ionization time of flight (MALDI-TOF) mass spectrometry. MALDI-TOF mass spectrometry was

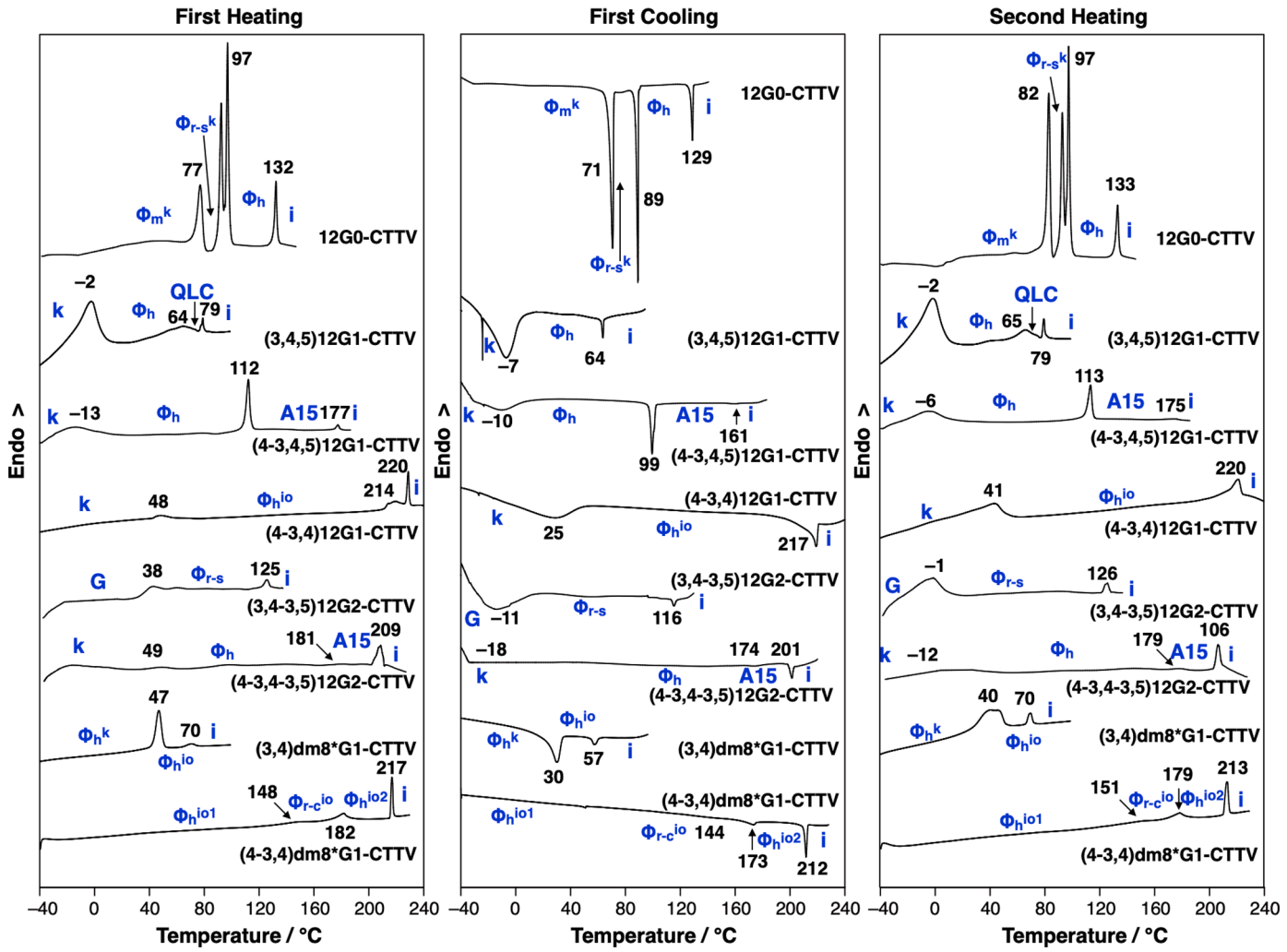

Fig. 2. DSC traces of *n*-alkylated and dendronized CTTV.

performed on PerSeptive Biosystems-Voyager-DE (Framingham, MA) mass spectrometer equipped with a nitrogen laser (337 nm) and operating in linear mode. Internal calibration was performed using Angiotensin II, and Bombesin as standards. The analytical samples were obtained by mixing THF solution of the sample (5–10 mg/mL), and the matrix (2,5-dihydroxybenzoic acid) (10 mg/mL) in a 1:1 to 1:5 v/v ratio. The prepared solution (0.5 μL) was loaded on the MALDI plate and allowed to dry at 25 °C before the plate was inserted into the vacuum chamber of the MALDI instrument.

Differential scanning calorimetry (DSC). Thermal transitions and their associated enthalpy changes were determined on a TA Instruments Q100 differential scanning calorimeter (DSC) equipped with a refrigerated cooling system at 10 °C min^{-1} heating and cooling rates. Indium was used as calibration standard. The transition temperatures were calculated as the maxima and minima of their endothermic and exothermic peaks.

Melting points. Melting points were measured using a uni-melt capillary melting point apparatus (Arthur H. Thomas Company) and were uncorrected.

Thermal optical polarized microscopy (TOPM). The texture was recorded by an Olympus BX51 optical microscope (100× magnification) equipped with a Mettler FP82HT hot stage and a Mettler Toledo FP90 Central Processor was used to verify thermal transitions.

X-ray diffraction (XRD). X-ray diffraction (XRD) measurements were performed using Cu-Kα1 radiation (λ = 1.542 Å) from a Bruker-Nonius FR-591 rotating anode X-ray source equipped with a 0.2 × 0.2 mm^2 filament and operated at 3.4 kW. Osmic Max-Flux optics, and triple pinhole collimation were used to obtain a highly collimated beam with a 0.3 × 0.3 mm^2 spot on a Bruker-AXS Hi-Star multiwire area detector. To minimize attenuation, and background scattering, an integral vacuum was maintained along the length of the flight tube, and within the sample chamber. Samples were held in glass capillaries (1.0 mm in diameter), mounted in a temperature-controlled oven (temperature precision: ± 0.1 °C, temperature range from –10 to 210 °C). Aligned samples for fiber XRD experiments were prepared using a custom-made extrusion device [57]. The powdered sample (~10 mg) was heated inside the extrusion device. After slow cooling, the fiber was extruded in the liquid crystal phase, and cooled to 23 °C. Typically, the aligned samples have a thickness of 0.3–0.7 mm, and a length of 3–7 mm. All XRD measurements were performed with the aligned sample axis perpendicular to the beam direction. Primary XRD analysis was performed using Datasqueeze (version 3.0.5) [83].

Molecular modeling. Molecular modeling, and simulation experiments were performed using Material Studio Modeling (version 5) software from Accelrys. The Forcite module was used to perform the energy minimizations on the supramolecular structures. Correct models must match the experimental density, the lattice dimensions and the original XRD data.

Results and discussion

Fig. 1 outlines the synthesis of $CTV(OMe)_6$ and of $CTTV(OMe)_8$ by

Table 1
Thermal analysis of selected dendronized CTTV, CTV, triphenylene (Tp), and 1,3,5-trihydroxylbenzene (THB) molecules, and their phase transition temperatures and enthalpy changes.

Compound	n [a]	Phase transition	T (heat) [b](°C)	T (cool) [c](°C)	ΔT [d](°C)	ΔH [e](kcal•mol^{-1})
(3,4,5)12G1-CTTV	8	Φ_h – QLC – i	64, 79	N/A, 64	N/A,15	N/A, 0.65
(3,4,5)12G1-CTV [f]	6	Φ_h – A15 – i	69, 93	60, 76	9,17	18.65, 0.67
(3,4,5)12G1-Tp [g]	6	Φ_h^{io} – σ – A15 – i	40, 96, 108	26, 86, 98	14, 10, 10	2.48, 0.43, 1.42
(4–3,4,5) 12G1-CTTV	8	Φ_h – A15 – i	112, 177	99, 161	13, 16	12.82, 0.88
(4–3,4,5) 12G1-CTV [f]	6	Φ_h^{io} – A15 – i	105, 187	N/A, 166	N/A, 21	N/A, 1.04
(4–3,4,5) 12G1-THB [i]	3	Φ_h – i	127	122	5	3.05
(4–3,4) 12G1-CTTV	8	Φ_h^{io} – i	220	217	3	6.60
(4–3,4) 12G1-CTV [f]	6	Φ_h – i	224	209	15	19.65
(4–3,4–3,5) 12G2-CTTV	8	A15 – i	209	201	8	6.94
(4–3,4–3,5) 12G2-Tp [h]	6	QLC – i	214	206	8	4.71
(3,4) dm8*G1-CTTV	8	Φ_h^{io} – i	70	57	13	1.20
(3,4) dm8*G1-CTV [h]	6	Φ_h – i	76	58	8	0.87
(4–3,4) dm8*G1-CTTV	8	Φ_h^{io} – i	217	212	5	3.62
(4–3,4) dm8*G1-CTV [h]	6	Φ_h – i	233	218	15	17.85

[a] Number of dendrons in the structure.
[b] Phase transition temperature upon heating.
[c] Phase transition temperature upon cooling.
[d] Differences between T (heat) and T (cool).
[e] Enthalpy of the phase transition.
[f] Data was published in Table 1 of Ref [33].
[g] Data was published in Table S1 of Ref [77].
[h] Data was published in Table 1 of Ref [34].
[i] Data was published in Table 1 of Ref [22]; Φ_h: *P6mm* hexagonal columnar liquid crystalline phase; io: intracolumnar order; A15: *Pm3n* simple cubic lattice; σ: $P4_2/mnm$ tetragonal lattice; QLC: Quasi-liquid crystals (12-fold); *i*: isotropic phase.

methods elaborated in our laboratory to generate predominantly the veratrole trimer CTV(OMe)$_6$ or veratrole tetramer CTTV(OMe)$_8$ respectively [80,81].

The different acids used in the electrophilic cyclization of veratrole, H_3PO_4 at 80–85 °C for trimerization and CF_3COOH at 0 °C for cyclotetramerization were responsible for the regiospecificity of this reaction [80]. The synthesis of CTV(OH)$_6$ and CTTV(OH)$_8$ was accomplished by demethylation of the corresponding methoxy precursors with BBr_3 in methylenechloride. The synthesis of *n*-alkylated and dendronized CTTV was accomplished by the etherification of CTTV(OH)$_8$ with the corresponding *n*-alkyl bromide or with the self-assembling dendron containing a benzyl chloride at the apex (Fig. 1). All CTTV derivatives were analyzed by DSC.

Their DSC traces are shown in Fig. 2 while transition temperatures collected from Fig. 2 together with their enthalpy changes and phases assigned by XRD are summarized in Tables 1, 2, and S1. Nomenclature of the dendrons and dendrimers was adapted from the previous publications in our laboratory [39] and is consistent with other publications, for example, CTV [33], Tp [34], and CTTV [73]. More specifically, **(3,4,5)12G1-CTTV** refers to the first generation (G1) dendron 3,4,5-tridodecyloxy benzyl [(3,4,5)12G1] on the periphery of CTTV.

A comparison of the transition temperature between the highest temperature self-organized phase and the isotropic liquid, known as isotropization temperature, T_i, on heating and cooling provides a qualitative indication between the flexibility of the system and its ability to reach an equilibrium state. Table 1 compares the T_i data available for all dendronized CTTV, THB [22], Tp [34] and CTV [33]. For the case of **12G0-CTTV** this difference in T_i is 3 or 4 °C, depending if the data are collected from the first or second heating scan (Fig. 2). This indicates that this compound undergoes a very fast transition that correlates with the fast dynamic of its CTTV core. Dendronized CTTVs exhibit a similarly small difference between T_i on heating and cooling for similar degrees of order of their assemblies. This is the case of **(4-3,4) 12G1-CTTV** (3 °C), **(4-3,4)dm8*G1-CTTV** (5 °C), **(3,4)dm8*G1-CTTV** (13 °C), **(3,4)dm8*G1-CTV** (8 °C), **(4-3,4-3,5)12G2-CTTV** (8 °C), **(4-3,4-3,5)12G2-Tp** (8 °C), **(4-3,4,5)12G1-CTTV** (16 °C), and **(4-3,4,5) 12G1-CTV** (21 °C) (Table 1).

The situation for **(3,4,5)12G1CTTV** (15 °C), **(3,4,5)12G1CTV** (75 °C), and **(3,4,5)12G1Tp** (10 °C) is more complex since for the case of CTTV, the highest temperature phase changes from A15 for CTV and Tp, to QLC for CTTV. This means the highest flexibility of CTTV changes not only the T_i but also the nature of the phase specially when the assembly is generated from spherical objects like in the case of **(3,4,5) 12G1CTTV** and **(3,4,5)12G1CTV**, as well as in the case of **(4-3,4-3,5) 12G2-CTTV** and **(4-3,4-3,5)12G2-Tp**. The elucidation of this sensible arrangement in which supramolecular spheres are self-organized, requires additional experiments. On increasing the order of the phase from the highest temperature from Φ_h or Φ_h^{io} to A15 or to QLC a small increase in this supercooling process was observed (Fig. 2 and Tables 1, S1). It is instructive to compare the T_i values of the more rigid but also monodisperse structures at the apex such as THB [22], Tp [34] and CTV [33]. In all cases more rigid structures at the apex provide higher T_i values and higher degrees of supercooling. This trend is also valid for H-bonding mediated structures at the apex (all libraries including dendritic dipeptides [1,23,24,84,86–90], crown ethers [47,50], DA interactions [46,91,92], salts [16], solvated salts [42,47,49–51,56,65]). It is also important to observe that dendronized CTV, CTTV and Tp undergo a transition from column to sphere forming assemblies (Fig. 2, Table 1) while dendronized CE and oligooxyethylenes including their complexes as well as polymers undergo a transition from column to elongated columns [42,47,49–51,56,65]. This is not a completely elucidated event considering that some lower molar mass dendronized polymers [62,63,70,71] undergo the column to sphere transition process. It is remarkable to observe that this small library (Fig. 1) provided a rare example of QLC (for **(3,4,5)12G1-CTTV**) and a Frank-Kasper A15 phase (for **(4-3,4,5)-12G1-CTTV**) but no σ phase. We are certain that additional experiments will also uncover the Frank-Kasper σ phase in CTTV derivatives.

A similar trend as that observed from DSC (Fig. 2) was obtained from the thermal optical polarized microscopy (TOPM) micrographs shown in Fig. 3. Equilibrium textures were observed regardless of if the side groups of CTTV are *n*-alkyl or self-assembling dendrons as long as the same phase is investigated by TOPM.

Tables 2 and S1 summarize the range of temperatures, the d-spacings, their assignments and lattice dimensions of all phases as obtained by using oriented-fiber XRD experiments. Some representative examples of oriented fiber XRDs are shown in Fig. 4 with the corresponding models in Figure S1. DSC traces of **12G0-CTTV** (Fig. 2, Table 1) indicate three phases before isotropization at 132 °C. Below 77 °C, there is a crystalline columnar monoclinic phase (Φ_m^k: *P*2). From 77 to 97 °C, a

Table 2
Structural analysis of the supramolecular dendrimers self-assembled from dendronized CTTV.

Supramolecular Dendrimers	T (°C)	Phase [a]	*a, b, c* (Å) [b]	ρ (g•cm^{-3}) [c]	M_{wt} (g•mol^{-1}) [d]	*t* (Å) [e]	μ [f]	D_{col} (Å) [g]/D_{sph} (Å)[g1]	d_{100}, d_{010}, d_{110}, d_{200}, d_{020}, d_{220}, d_{2-20}, d_{230}, d_{400}, d_{420} (Å) [h] d_{100}, d_{010}, d_{110}, d_{210}, d_{310}, d_{320}, d_{410}, d_{500} (Å) [i] d_{00002}, d_{12100}, d_{10102}, d_{12101}, d_{12103} (Å) [j] d_{100}, d_{110}, d_{200}, d_{210}, d_{300} (Å) [k] d_{200}, d_{210}, d_{211}, d_{310}, d_{320}, d_{222}, d_{321}, d_{400} (Å) [l] d_{200}, d_{100}, d_{010}, d_{110}, d_{300} (Å) [m] d_{110}, d_{020}, d_{200}, d_{130}, d_{220}, d_{040}, d_{001} (Å) [n]
12G0-CTTV	25	Φ_m[k]	25.0, 22.0, 4.8 [§]	1.04	1835.1	4.8	0.9 ~ 1	22.0	24.9, 21.9, 17.6, 12.4, 10.9, 9.3, 7.7, 6.9, 6.1, 5.8 [h]
	85	$\Phi_{r\text{-}s}$[k]	26.5, 23.8, 4.8 [§]			4.8	1.0 ~ 1	23.8	27.0, 23.3, 18.8, 11.7, 8.3, 7.2, 6.4, 5.4 [i]
	105	Φ_h[io]	28.9, 28.9, 4.8 [§]			4.8	1.1 ~ 1	28.9	25.1, 14.5, 12.6 [k]
(3,4,5)12G1-CTTV	30	Φ_h	30.1, 30.1, – [§]			4.9	1.1 ~1	30.1	26.1, –, –, –, – [k]
	70	**QLC**	68.5, 68.5, 68.5	0.97	5633.2	–	5.6 ~ 6	46.8[g1]	34.4, 31.6, 29.9, 28.7, 18.5 [j]
(4–3,4,5)12G1-CTTV	70	Φ_h	46.3, 46.3, – [§]	1.01	8180.2	4.8	1.0 ~ 1	46.3	40.2, 23.1, 20.1, –, –,– [k]
	125	**A15**	84.9, 84.9, 84.9			–	5.7 ~ 6	52.7 [g1]	42.7, 37.9, 34.6, –, 23.5, – 22.6,21.1 [l]
(4–3,4)12G1-CTTV	80	Φ_h[io]	43.0, 43.0, 4.9 [§]	1.04	5856.5	4.9	0.8 ~ 1	43.0	37.4, 21.5, 18.7, –, – [k]
(3,4–3,5)12G2-CTTV	50	Φ_h	39.9, 23.0, – [§]	0.98	8806.8	–	0.8 ~ 1	46.1	39.9, 23.0, 20.1, –, – [k]
(4–3,4–3,5) 12G2-CTTV	100	Φ_h	41.0, 41.0, – [§]	1.07	12,202	–	0.9 ~ 1	41.0	35.3, 20.6, 17.7, 13.4, 11.8 [k]
	190	**A15**	73.2, 73.2, 73.2	1.07		–	6.7 ~ 7	45.4[g1]	51.2, 36.5, 32.7, 29.9, –, 26.0, –, – [l]
(3,4)dm8*G1-CTTV	15	Φ_h[k]	36.0, 36.0, 44.0 [§]	1.01	3709.8	5.5	1.0 ~ 1	36.0	31.2, 18.0, 15.6, 11.8, 10.4 [k]
	60	Φ_h[io]	34.4, 34.4, 34.4 [§]			–	5.8 ~ 6	34.4	29.8, 17.2, 14.9, 11.3, 9.5 [k]
(4–3,4)dm8*G1-CTTV	100	Φ_h[io1]	43.0, 43.0, 4.9 [§]	1.04	5407.8	4.9	0.9 ~ 1	43.0	37.3, 21.1, 18.6, –, – [k]
	85	$\Phi_{r\text{-}c}$[io]	70.4, 46.0, 4.9 [§]			4.9	1.8 ~ 2	40.4	38.6, 35.2, 23.0, 20.9, 19.3, 17.6 [m]
	105	Φ_h[io2]	41.3, 41.3, 4.9 [§]			4.9	0.8 ~ 1	41.3	35.8, 20.7, 17.9, –, – [k]

[a] Φ_m[k]: ***P2*** crystalline monoclinic phase, $\Phi_{r\text{-}s}$[k]: ***P2mm*** crystalline simple rectangular columnar phase, Φ_h[io], ***P6mm*** Liquid crystalline columnar hexagonal phase with intracolumnar order. **QLC:** Quasi-liquid crystals (12-fold); Φ_h**:** ***P6mm*** hexagonal columnar lattice; **A15:***Pm*$\bar{3}$*n*simple cubic lattice; Φ_h[k]**:** ***P6mm*** crystalline hexagonal phase; $\Phi_{r\text{-}c}$[io], ***C2mm*** Simple rectangular columnar liquid crystalline phase.

[b] Lattice parameters (with uncertainty of ~1%).

[c] Experimental density (ρ) measured at room temperature (24 ºC).

[d] Molecular weight (M_{wt}) of the compound.

[e] Stratum thickness calculated from the VWAXS pattern.

[f] Average number of molecules in the unit cell of columnar phases, calculated using $\mu = N_A\, A\, t\, \rho\, /\, M_{wt}$ where $N_A = 6.022 \times 10^{23}$ mol^{-1} = Avogadro's number, A is the area of the column cross-section calculated from the lattice parameters and ρ is the density. Average number of dendrimers forming a sphere of the unit cell of a **QLC** phase $\mu = (a^3 N_A \rho)/6M_{wt}$ and **A15** phase is $\mu = (a^3 N_A \rho)/8M_{wt}$ where *a* is the lattice parameter, M_{wt} is the molecular weight, $N_A = 6.022 \times 10^{23}$ mol^{-1} = Avogadro's number, ρ is the density of the compound.

[g] Column diameter: for Φ_h phase $D_{col} = a$, for $\Phi_{r\text{-}s}$, $\Phi_{r\text{-}c}$ and Φ_m phase, lattice dimensions *a* and *b* are given; for the Cubic **A15** phase and **QLC** phase $a = b = c$. [g1] Sphere diameter calculated for the **A15** phase using $D_{sphere} = 2(3a^3/32\pi)^{1/3}$ and for the $\mathbf{QLC_{12\text{-}fold}}$ phase $[D_{sph} = 2a/(8\pi)^{1/3}$.

[h] Experimental diffraction peaks *d*-spacing for Φ_m phase.

[i] Experimental diffraction peaks *d*-spacing for $\Phi_{r\text{-}s}$ phase.
[j] Experimental diffraction peaks *d*-spacing for Φ_h phase.
[k] Experimental diffraction peaks *d*-spacing for **A15** phase.
[l] Experimental diffraction peaks *d*-spacing for ***P2mm*** phase.
[m] Experimental diffraction peaks *d*-spacing for $\Phi_{r\text{-}c}$ phase.
[§] This is fiber direction.

simple rectangular crystalline columnar phase ($\Phi_{r\text{-}s}^{k}$: *P2mm*) is observed. From 97 °C to its isotropic point (132 °C), a hexagonal columnar liquid crystalline phase with intracolumnar order (Φ_h^{io}: *P6mm*) is seen.

Characteristic very wide-angle powder X-ray diffraction patterns (VWAXS) at 25 °C for **12G0-CTTV** and their corresponding radial plots at 25 °C are shown in Fig. 4a–c and have been summarized in Table 2. XRD patterns (Fig. 4a) and corresponding radial plot (Fig. 4b) at 25 °C indicate that it is a Φ_m^{k} phase. The lattice parameters at 25 °C are determined to be $a = 25.0$, $b = 22.0$ Å, $c = 4.8$ Å, and $\gamma = 82.7°$. Measured d-spacings at 25 °C are $d_{100} = 24.9$ Å, $d_{010} = 21.9$ Å, $d_{110} = 17.6$ Å, $d_{200} = 12.4$ Å, $d_{020} = 10.9$ Å, $d_{220} = 9.3$ Å, $d_{2\text{–}20} = 7.7$ Å, $d_{230} = 6.9$ Å, $d_{400} = 6.1$ Å, $d_{420} = 5.8$ Å, and $d_{001} = 4.8$ Å (Table 2). VWAXS at 85 °C for **12G0-CTTV** and their corresponding radial plots at 85 °C is shown in Fig. 4d and have been summarized in Table 2. XRD patterns (Fig. 4d) and corresponding radial plot (Fig. 4e) at 85 °C indicate that it is $\Phi_{r\text{-}s}^{k}$. The lattice parameters at 85 °C are determined to be $a = 26.5$, $b = 23.8$ Å, and $c = 4.8$ Å. Measured d-spacings at 85 °C are $d_{100} = 27.0$ Å, $d_{010} = 23.3$ Å, $d_{110} = 18.8$ Å, $d_{210} = 11.7$ Å, $d_{310} = 8.3$ Å, $d_{320} = 7.2$ Å, $d_{410} = 6.4$ Å, $d_{500} = 5.4$ Å (Table 2). VWAXS at 105 °C for **12G0-CTTV** and their corresponding radial plots at 105 °C are shown in Fig. 4g and have been summarized in Table 2. XRD patterns (Fig. 4g) at 105 °C indicate that this is a Φ_h^{io} phase. The lattice parameters at 105 °C are $a = 28.9$, $b = 28.9$ Å, and $c = 4.8$ Å. Measured d-spacings at 105 °C are $d_{100} = 25.1$ Å, $d_{110} = 14.5$ Å, $d_{200} = 12.6$ Å, $d_{001} = 4.8$ Å (Table 2).

From the known molecular weight (M_{wt}) 1835.1 g.mol^{-1}, we determined the average number of dendrimers forming the supramolecular column stratum to be equal to one molecule per stratum ($\mu = 0.9 \sim 1$ for Φ_m^{k} phase, $\mu = 1.0 \sim 1$ for $\Phi_{r\text{-}s}^{k}$ phase, $\mu = 1.1 \sim 1$ for Φ_h^{io} phase). The column diameter (D_{col}) is 22.0 Å for Φ_m^{k} phase, 23.8 Å for $\Phi_{r\text{-}s}^{k}$ phase, and 28.9 Å for Φ_h^{io} phase (Table 2). Figure S1 shows the molecular models for Φ_m^{k}, $\Phi_{r\text{-}s}^{k}$, and Φ_h^{io} phases. The repeat unit is formed by one molecule for all the phases (Fig. S1a, b) and the column is formed in a similar way with an average strata distance of 4.8 Å. In the first step, one molecule is placed with a distorted CTTV core (Fig. S1a, b). In the second step, another molecule is placed at an average distance 4.8 Å (Fig. S1d).

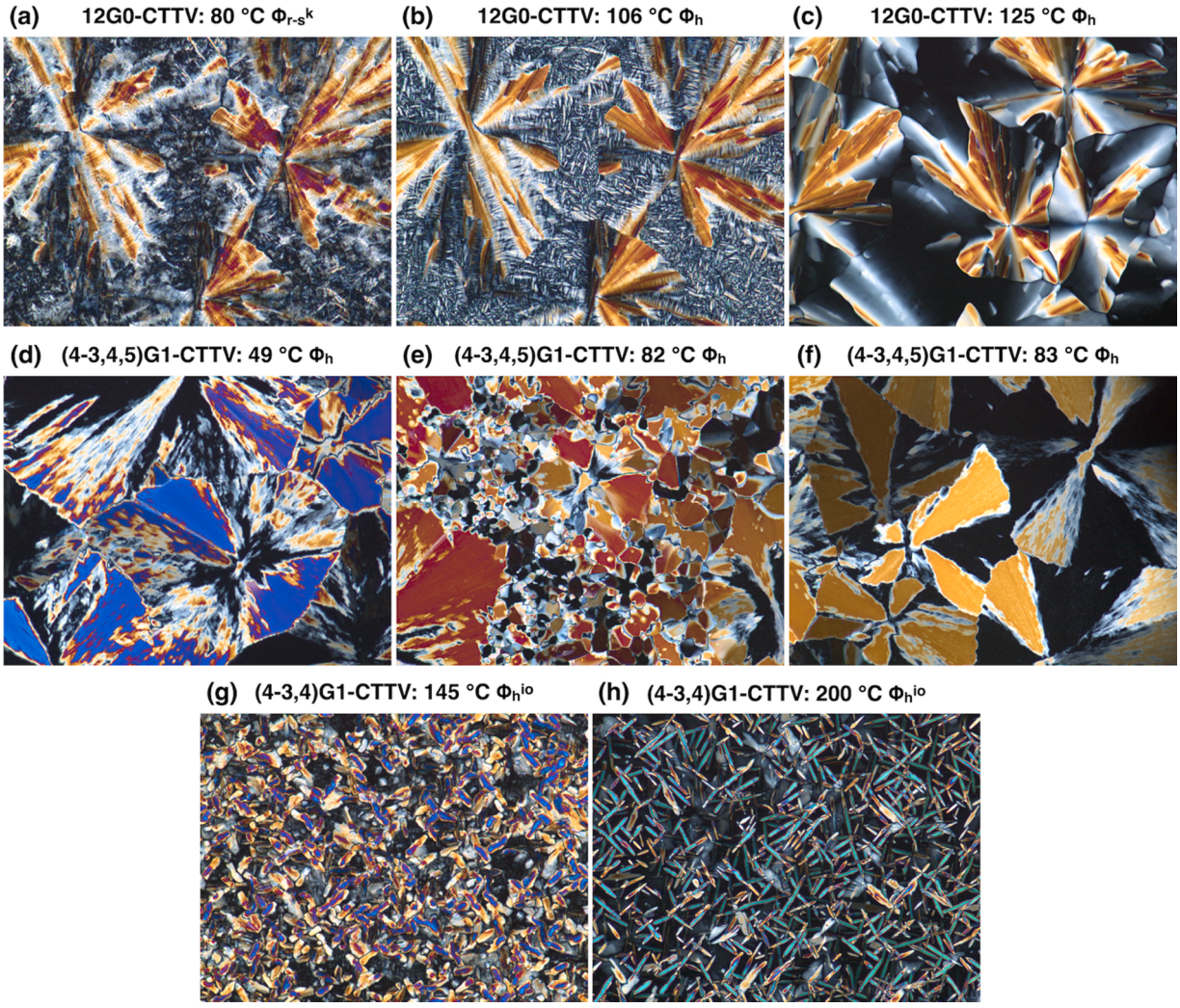

Fig. 3. Thermal optical polarized micrographs (TOPMs) of dendronized CTTV of **12G0-CTTV** (a–c), **(4-3,4,5)12G1-CTTV** (d–f), and **(4-3,4)12G1-CTTV** (g, h) at indicated temperatures.

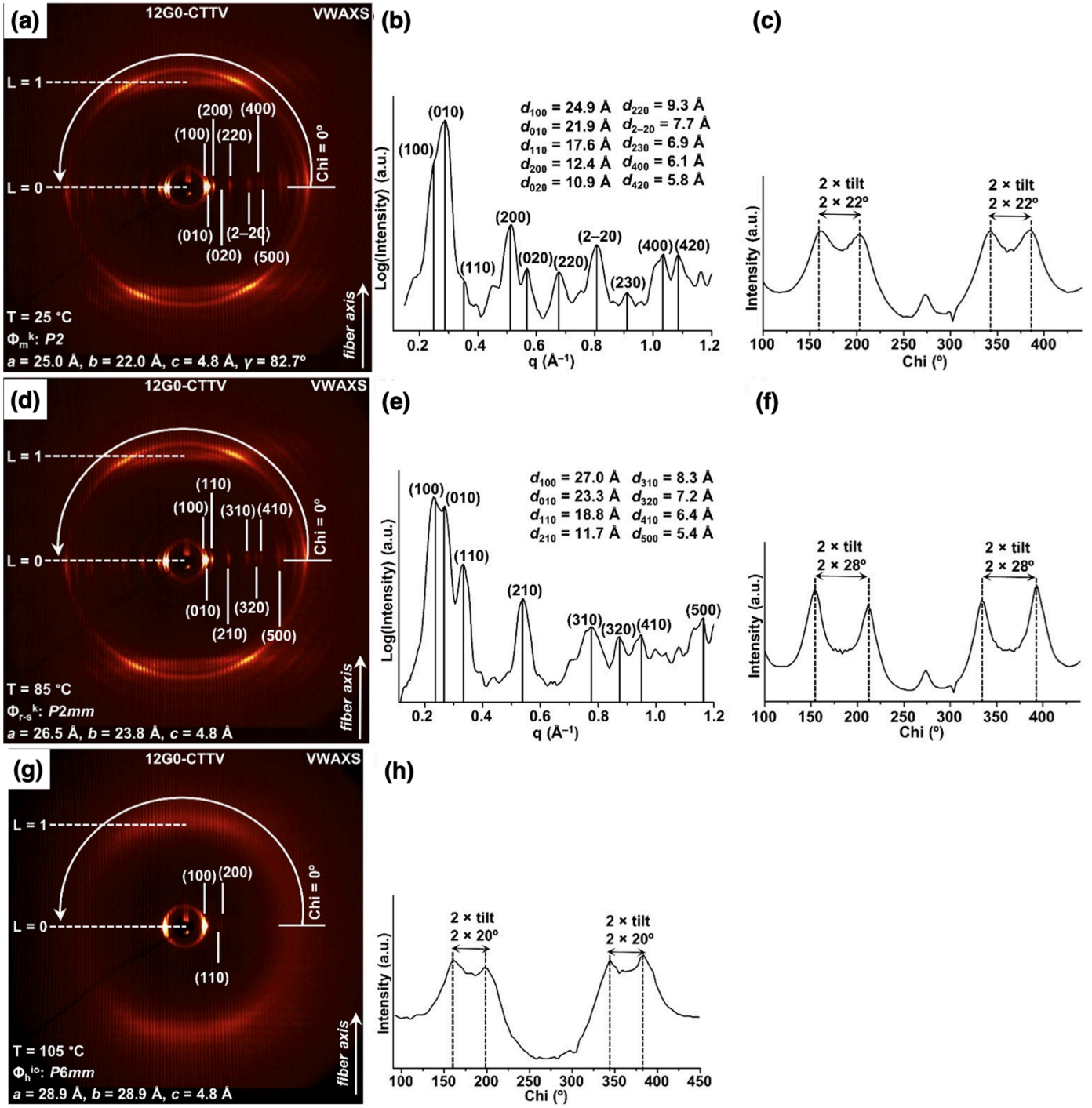

Fig. 4. (a) Very wide-angle fiber XRD (VWAXS) pattern (Φ_m^k: *P*2 phase) of **12G0-CTTV** collected at 25 °C during first heating. Diffraction indexes, fiber axis and lattice parameters are indicated. (b) Corresponding radial plot indicating the Φ_m^k: *P*2 phase. d-Spacings are shown. (c) Azimuthal plot [Intensity (a.u.) vs. Chi (°)] from the XRD pattern at 25 °C illustrating the tilting feature. (d) VWAX pattern ($\Phi_{r\text{-}s}^k$: *P2mm* phase) of **12G0-CTTV** collected at 85 °C during first heating. Diffraction indexes, fiber axis and lattice parameters are indicated. (e) Corresponding radial plot indicating the $\Phi_{r\text{-}s}^k$: *P2mm* phase. d-Spacings are shown. (f) Azimuthal plot [Intensity (a.u.) vs. Chi (°)] from the XRD pattern at 85 °C illustrating the tilting feature. (g) VWAX pattern (Φ_h^{io}: *P6mm* phase) of **12G0-CTTV** collected at 105 °C during first heating. Diffraction indexes, fiber axis and lattice parameters are indicated. (h) Azimuthal plot [Intensity (a.u.) vs. Chi (°)] from the XRD pattern at 105 °C illustrating the tilting feature.

Thus, a column structure is formed (Fig. S1d). These columns will arrange themselves in a monoclinic array (Fig. S1e), in a simple rectangular array (Fig. S1f), and in a hexagonal array (Fig. S1g). VWAXS (Fig. 4) indicates the tilting angle of the alkyl groups with the columnar axis [22° for Φ_m^k phase (Fig. 4c), 28° $\Phi_{r\text{-}s}^k$ phase (Fig. 4f), and 20° Φ_h^{io} phase (Fig. 4h)].

Fig. 5 shows a representative XRD of the QLC phase of **(3,4,5)12G1-CTTV**. In contrast, the corresponding dendronized molecules with CTV and Tp at the apex showed A15 or σ phases (Table 1) [30,31]. DSC traces (Fig. 2, Table S1) indicate that **(3,4,5)12G1-CTTV** displays three phases. XRD patterns were used to determine them. Below –2 °C, there is an unknown crystalline phase (*k*). From –2 °C to 64 ° C, a Φ_h phase is found. From 64 to 79 °C, a QLC phase is observed. At 79 °C, this phase reaches the isotropization temperature (*i*).

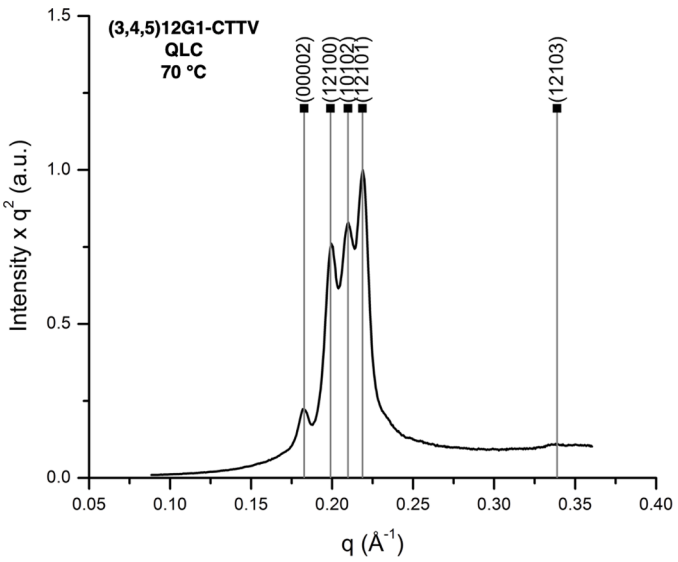

Fig. 5. Small angle powder diffraction pattern collected at 70 °C from **(3,4,5)12G1-CTTV** self-organized into the QLC.

XRD patterns at 30 °C for **(3,4,5)12G1-CTTV** have been summarized in Table 2. XRD patterns at 30 °C indicates a Φ_h phase. Lack of off axis diffraction pattern suggests that this phase is a 2D hexagonal lattice. The lattice parameters at 30 °C are determined to be $a = 30.1$ and $b = 30.1$ Å. The measured d-spacings at 30 °C are $d_{100} = 26.1$ Å (Table 2). From the known molecular weight (M_{wt}) 5633.2 g.mol^{-1}, we calculated the average number of dendrimers forming the supramolecular column stratum. We find that in both Φ_h phases, there must be one molecule ($\mu = 1.1 \sim 1$ for Φ_h) per column cross-section. The column diameter is 30.1 Å for Φ_h phase [$D_{col} = a$]. The *c*-axis of the Φ_h phase is along the fiber axis. Figure S2a–e displayed the molecular models of the Φ_h phase. For the Φ_h phase, the repeat unit is formed by one molecule per stratum (Fig. S2a–c). In the first step, one molecule is placed with highly distorted CTTV core (Fig. S2a, b). In the second step, another molecule is placed on top of the first molecule at 4.9 Å (Fig. S2c, d). Thus, each molecule will stack over one another to assemble the supramolecular column (Fig. S2c, d) and thus these columns will arrange themselves in a hexagonal array (Fig. S2e). Small angle XRD patterns (SAXS) (Fig. 5) at 70 °C indicate that this phase is QLC. The lattice parameters at 30 °C are determined to be $a = b = c = 68.5$ Å. Measured d-spacings at 30 °C are $d_{00002} = 34.4$ Å, $d_{12100} = 31.6$ Å, $d_{10102} = 29.9$ Å, $d_{12101} = 28.7$ Å, and $d_{12103} = 18.5$ Å (Table 2). From the known molecular weight (M_{wt}) 5633.2 g.mol^{-1}, we calculate the average number of dendrimers forming the unit cell of the QLC phase to be about 34 molecules in a unit cell. Therefore, each sphere in the QLC phase is formed by six molecules. Hence, we calculate the number of molecules (μ) constructing the sphere which is 6 [$\mu = \mu'/6$, $\mu = 5.6 \sim 6$] in a sphere. The sphere diameter is 46.8 Å for the QLC phase [$D_{sph} = 2a/(8\pi)^{1/3}$] (Table 2). The models of the sphere which form the QLC lattice are shown in Fig. S2f, g. The sphere is formed by six molecules. The CTTV cores of the six molecules placed in a similar way as in the columns of the hexagonal phase. But the phenyl rings and the alkyl groups are much more disordered to form a sphere. Fig. S2f and S2g represent the top view and the side view respectively. A schematic representation of the QLC lattice is provided in Fig. S2h.

DSC traces (Fig. 2, Table S1) of the supramolecular dendrimer of **(4-3,4)12G1-CTTV** indicate that it exhibits two phases before its isotropization at 220 °C. During the first heating (Fig. 2), a small hump is found before the isotropization (from 214 to 220 °C), but because of very small temperature range (~ 6 °C) the phase could not be determined. Interesting the hump does not appear during the cooling or subsequent heating and cooling. Below 48 °C, there is an unknown crystalline phase (*k*). A Φ_h^{io} phase is observed between 48 and 220 °C during the first heating. VWAXS and their corresponding radial plots at 80 °C are shown in Fig. 6 and have been summarized in Table 2. The lattice parameters at 80 °C are determined to be $a = b = 43.0$ Å, $c = 4.9$ Å. Measured d-spacings are $d_{100} = 37.4$ Å, $d_{110} = 21.5$ Å, $d_{200} = 18.7$ Å, $d_{001} = 4.9$ Å (Table 2). The absence of off-axis features (Fig. 6a) in VWAX XRD pattern indicates that it is a liquid crystalline phase. From the known molecular weight (M_{wt}) 5856.5 g.mol^{-1}, we infer an average number of dendrimers forming the supramolecular column stratum to be one molecules ($\mu = 0.8 \sim 1$) per stratum. The column diameter is 43.0 Å [$D_{col} = a$]. The *c*-axis of this hexagonal phase is along the fiber axis. The molecular model for the Φ_h^{io} phase is shown in Fig. S3. The repeat unit is formed by one molecule (Fig. 3c). In the first step, one molecule is placed with a distorted CTTV core (Fig. S3a–c). In the second step, another molecule is placed on top of the first molecule at 4.9 Å (Fig. S3d–g). Thus, each molecule will stack over one another to form the supramolecular column of the Φ_h^{io} phase (Fig. 3d–g). These columns, therefore, arrange themselves in a hexagonal array (Fig. S3f). The Intensity (a.u.) vs. Chi (°) plot (Fig. 6d) indicates that the alkyl groups are tilted by 27° with the column axis.

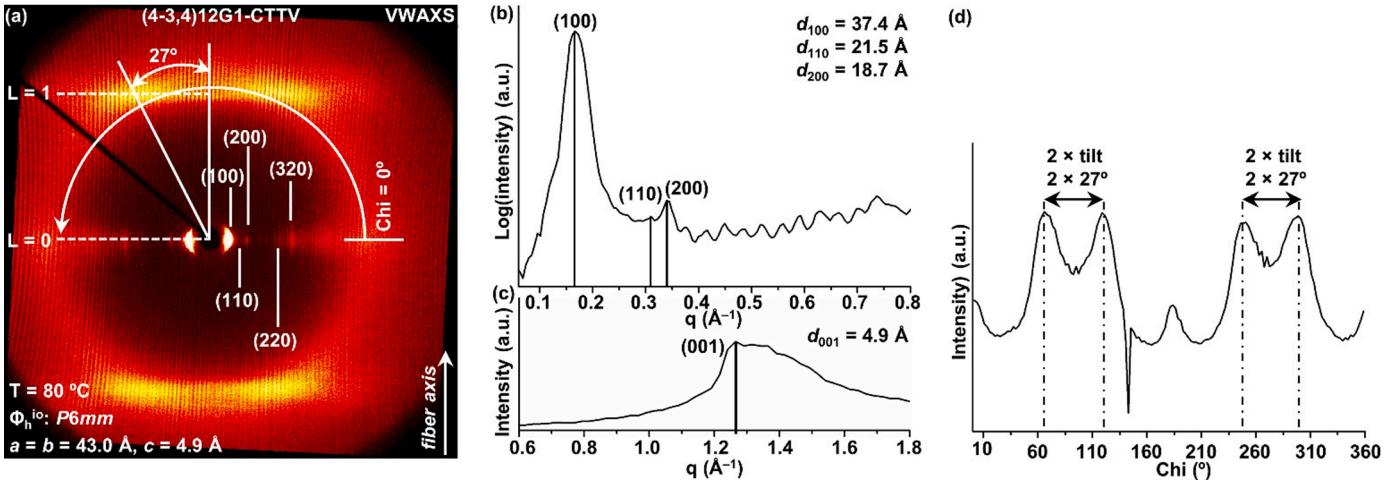

Fig. 6. (a) Very wide-angle XRD pattern (VWAXS) of **(4-3,4)12G1-CTTV** at 80 °C. (100), (110), (200), (220), and (320) diffractions indicate a (Φ_h^{io} phase. Diffraction indexes, fiber axis, tilting feature, and lattice parameters are indicated. (b) Radial plot along the equatorial plane from the XRD pattern. d-Spacings are shown. (c) Radial plot along the meridional axis from the XRD. d-Spacing is shown. (d) Intensity (a.u.) vs. Chi (°) plot from the XRD pattern illustration the tilting features of the alkyl groups (–$C_{12}H_{25}$).

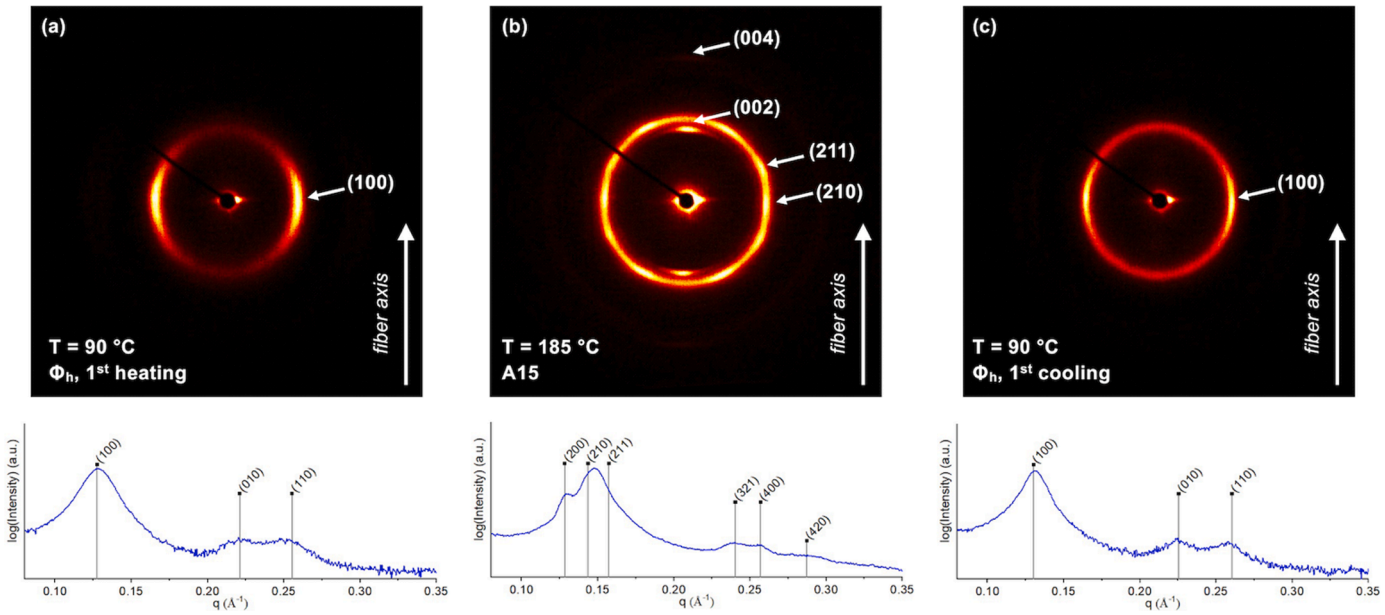

Fig. 7. Small angle fiber diffraction pattern from **(4-3,4-3,5)12G2-CTTV** self-organized into Φ_h upon first heating (a), A15 phase (b), and into Φ_h upon first cooling (c).

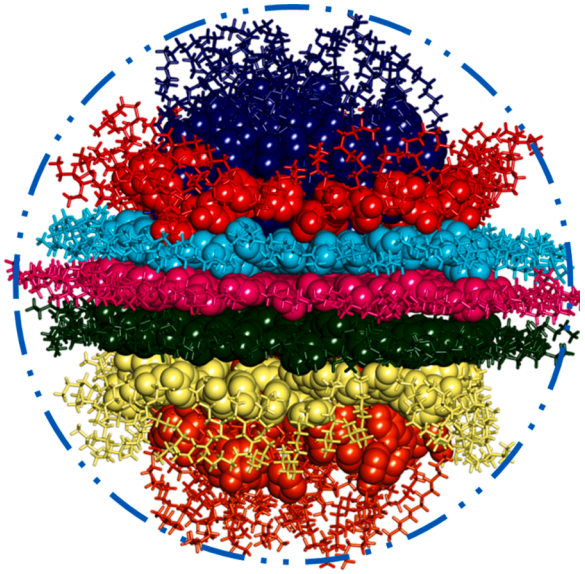

Fig. 8. Mechanism of formation of the supramolecular sphere of the A15 phase of **(4-3,4-3,5)12G2-CTTV**.

The DSC traces (Fig. 2, Table S1) indicate that **(3,4-3,5)12G2-CTTV** exhibits two phases before isotropization at 125 °C. Below 38 °C, there is a glassy (*G*) phase. From 38 to 125 °C, a Φ_h phase is found. At 125 °C, the compound reaches the isotropic point (*i*). Characteristic X-ray diffraction patterns at 50 °C for **(3,4-3,5)12G2-CTTV** have been summarized in Table 2. XRD patterns 50 °C and the radial plots indicates that it is a Φ_h phase. Lack of off axis diffraction pattern indicates that it is a 2D hexagonal phase. The lattice parameters at 50 °C are determined to be $a = b = 46.1$ Å. Measured d-spacings at 50 °C are $d_{100} = 39.9$ Å, $d_{110} = 23.0$ Å, and $d_{200} = 20.1$ Å (Table 2). From the known molecular weight (M_{wt}) 8806.8 g.mol^{-1}, we determined an average number of dendrimers forming the supramolecular column stratum must be one molecule ($\mu = 0.8 \sim 1$) per stratum. The column diameter is 46.1 Å [$D_{col} = a$]. The *c*-axis of the phase is along the fiber axis. Figure S4a–d displays the molecular models for Φ_h phase. For Φ_h phase the repeat unit is formed by one molecule (Fig. S4a, b). In the first step, one molecule is placed with highly distorted CTTV core (Fig. S4a, b). In the second step, another molecule is placed on top of the first molecule at 4.9 Å (Fig. S4c, d). Thus, each molecule will stack over one another to form the column (Fig. S4c, d) and thus these supramolecular columns will arrange themselves in a hexagonal array.

The oriented fiber XRD from Fig. 7 demonstrated that **(4-3,4-3,5)12G12-CTTV** forms Φ_h and A15 phases but did not show a supramolecular orientational memory (SOM) effect [74–79]. In contrast, **(4-3,4,5)12G12-CTTV** was reported to show an orthogonal SOM [77] effect when cooled from A15 to Φ_h phase. SOM was discovered in our laboratory [74–79]. It represents a special case of epitaxial orientation when oriented fibers of self-assembling dendrimers generated in the Φ_h phase maintain the orientation of an A15, body-central cubic (BCC) or σ phase upon cooling back to the Φ_h phase from the sphere forming supramolecular assemblies. This event generates a large diversity of novel morphologies that are not accessible by any other mechanism [74–79].

DSC traces (Fig. 2, Table S1) indicate that **(4-3,4,5)12G1-CTTV** exhibits three distinguished phases before isotropization at 177 °C. Below –13 °C, there is an unknown crystalline phase. From –13 to 112 °C, a Φ_h phase is found. From 112 to 177 °C, a A15 phase is observed. At 177 °C, the A15 phase undergoes isotropization (*i*). Below –13 °C, the phase seems to be crystalline to be denoted as *k*. Characteristic X-ray diffraction patterns at 70 °C for **(4-3,4,5)12G1-CTTV** have been summarized in Table 2. XRD patterns 70 °C indicate that it is a Φ_h phase. The lattice parameters at 30 °C are determined to be $a = 46.3$ Å and $b = 46.3$ Å. Measured d-spacings at 70 °C are $d_{100} = 40.2$ Å, $d_{110} = 23.1$ Å, and $d_{200} = 20.1$ Å (Table 2). From the known molecular weight (M_{wt}) 8180.2 g.mol^{-1}, we determine the average number of dendrimers forming the supramolecular column stratum that is about one molecule ($\mu = 1.1 \sim 1$ for Φ_h. The column diameter is 46.3 Å for Φ_h phase [$D_{col} = a$]. The *c*-axis of the hexagonal phase is along the fiber axis. Fig. S5a–e shows the molecular models for the Φ_h phase. The repeat unit is formed by one molecule (Fig. S5a–c). For the Φ_h phases, in the first step, one molecule is placed with highly distorted CTTV core (Fig. S5a, b). In the second step, another molecule is placed on top of the first molecule at 4.9 Å (Fig. S5c, d). Thus, each molecule will stack over one another to form the column (Fig. S5c, d) and thus these columns will arrange themselves in a hexagonal array (Fig. S5e). WAXS at 125 °C indicate that the phase is A15. The lattice parameters at 125 °C are determined to be *a*

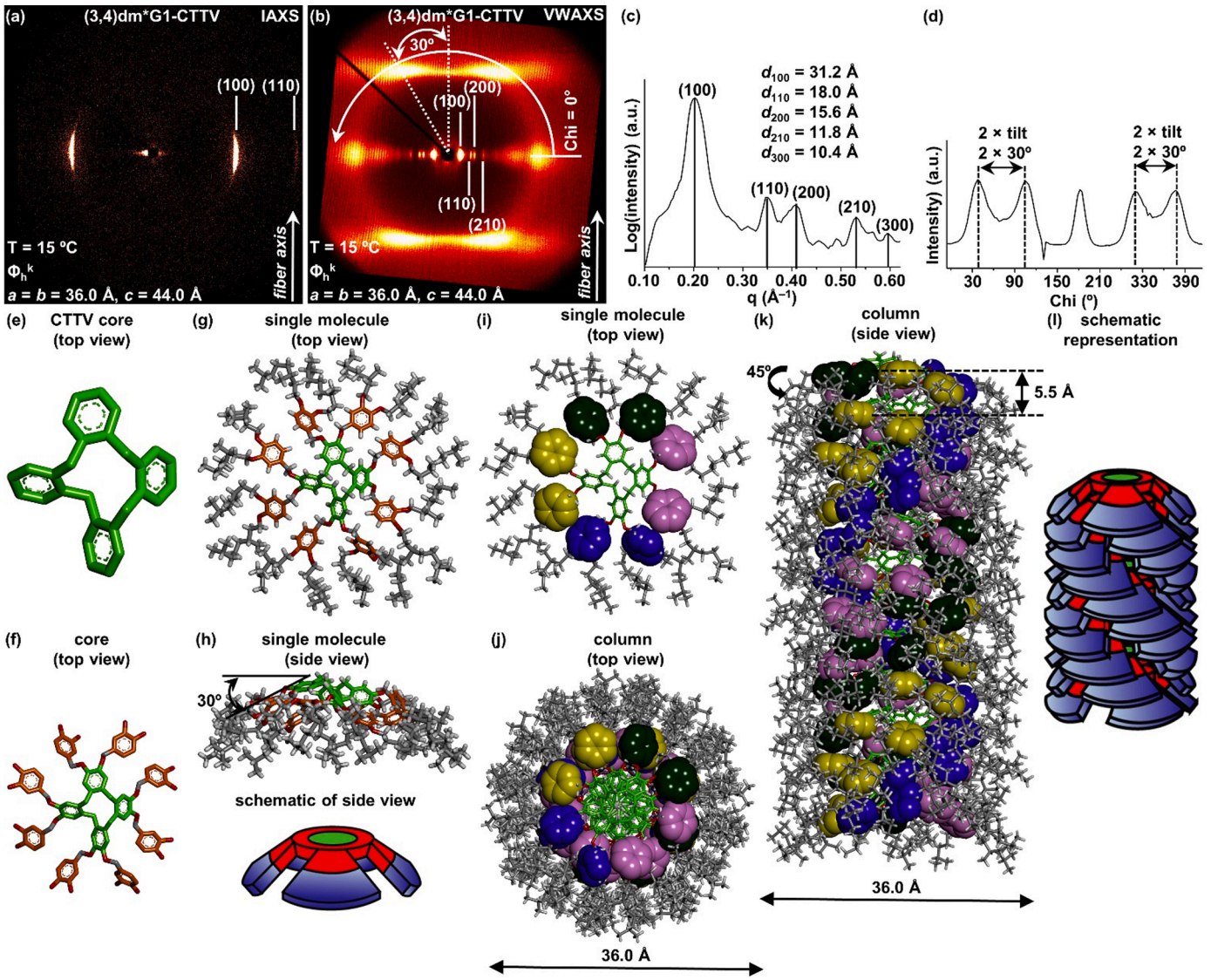

Fig. 9. (a) Intermediate-angle fiber XRD (IAXS) patterns (Φ_h^k phase) of **(3,4)dm8*G1-CTTV** at 15 °C. (b) VWAX patterns (Φ_h^k phase) of **(3,4)dm8*G1-CTTV** at 15 °C. Diffraction indexes, fiber axis and lattice parameters are indicated. (c) Radial plot along the equatorial plane showing the (100), (110), (200), (210), and (300) diffractions indicating a hexagonal phase. d-spacings are shown. (d) Azimuthal plot [Intensity (a.u.) vs. Chi (°)] from the VWAXS XRD pattern illustrating the tilting feature. (e–k) Molecular models for the (Φ_h^k phase) of **(3,4)dm8*G1-CTTV** at 15 °C; (e) Twisted and distorted CTTV core (top view); (f) CTTV core with the phenyl rings (top view); H-atoms have been omitted for clarity in e–f. (g) Single molecule (top view); (h) Single molecule showing the tilting feature (side view); (i–k) Rainbow color model; (i) Single molecule showing the color code (top view); (j) Column (colored, top view); (k) Column (colored, side view). (l) Schematic representation of the columns in the hexagonal array (side view). Color code used in the model (e–h): O atoms, red; H atoms, white; C atoms in the CTTV core, green; C atoms in the other phenyl rings, orange; all other C atoms, gray.

$= b = c = 84.9$ Å. Measured d-spacings at 125 °C are $d_{200} = 42.7$ Å, $d_{210} = 37.9$ Å, $d_{211} = 34.6$ Å, $d_{320} = 23.5$ Å, $d_{321} = 22.6$ Å, and $d_{400} = 21.1$ Å (Table 2). From the known molecular weight (M_{wt}) 8180.2 g.mol^{-1}, we infer that the average number of dendrimers forming a sphere of the unit cell should be 6 molecules (5.7 ~ 6) in a sphere. The sphere diameter is 52.7 Å for the A15 phase [$D_{sph} = 2(3a^3/(32\pi)^{1/3}$] (Table 2). The models of the sphere which form the A15 lattice is shown in Fig. S5f, g. The sphere is formed by six molecules. The CTTV cores of the six molecules placed in a similar way as in the columns of the hexagonal phase. But the phenyl rings and the alkyl groups are highly disordered to form a sphere. Fig. S5f and S5g represent the top view and the side view respectively. A schematic representation of the A15 lattice is provided in Fig. S5h.

DSC traces (Fig. 2, Table S1) indicate that **(4-3,4-3,5)12G2-CTTV** exhibits three phases before isotropization at 209 °C. Below 49 °C, there is an unknown crystalline phase (*k*). From 49 to 181 °C, a Φ_h phase is observed. From 181 to 209 °C, a A15 phase is available. At 209 °C, this phase undergoes isotropization (*i*). Characteristic X-ray diffraction patterns at 100 °C for **(4-3,4-3,5)12G1-CTTV** have been summarized in Table 2 and are shown in Fig. 7a. XRD patterns at 100 °C and the radial plots (Fig. 7) indicate that it is columnar liquid crystalline hexagonal phase (Φ_h phase). The lattice parameters at 100 °C are determined to be $a = b = 41.0$. Measured d-spacings at 100 °C are $d_{100} = 35.3$ Å, $d_{110} = 20.6$ Å, $d_{200} = 17.7$ Å, $d_{210} = 13.4$ Å and $d_{200} = 11.8$ Å (Table 2). From the known molecular weight (M_{wt}) 12,202.0 g.mol^{-1}, we determined the average number of dendrimers forming the supramolecular column stratum to be one molecule ($\mu = 0.9 \sim 1$) in the repeat unit of Φ_h phase. The column diameter is 41.0 Å [$D_{col} = a$]. The *c*-axis of the phase is along the fiber axis. Figure S6a–e consists of the molecular models for Φ_h phase. The repeat unit is formed by one molecule (Fig. S6a, b). In the first step, one molecule is placed with highly distorted CTTV core (Fig. S6a, b). In the second step, another molecule is placed on top of the first molecule at 4.9 Å (Fig. S6c, d). Thus, each molecule will stack over

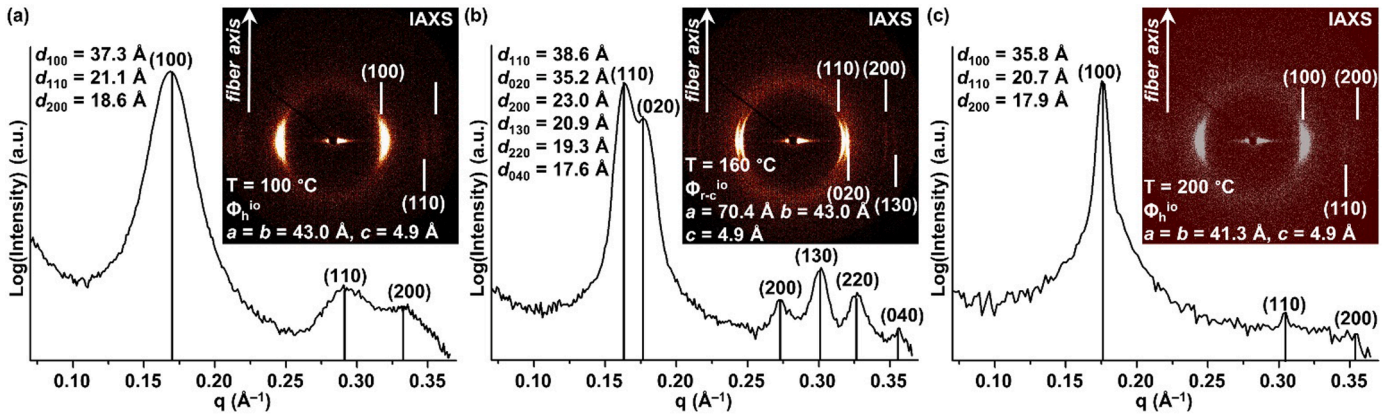

Fig. 10. (a) Radial plot along the equatorial plane from the IAXS of **(4-3,4)dm8*G1-CTTV** at 100 °C. (100), (110), and (200) diffractions indicate a columnar hexagonal phase. d-Spacings are shown. IAXS at 100 °C is shown in the inset. Diffraction indexes, fiber axis and lattice parameters are indicated. (b) Radial plot along the equatorial plane from IAXS of **(4-3,4)dm8*G1-CTTV** at 160 °C. (110), (020), (200), (130), (220) and (040) diffractions indicate a centered rectangular phase. d-Spacings are shown. Intermediate-angle XRD pattern (IAXS) at 160 °C is shown in the inset. Diffraction indexes, fiber axis and lattice parameters are indicated. (c) Radial plot along the equatorial plane from IAXS of **(4-3,4)dm8*G1-CTTV** at 200 °C. (100), (110), and (200) diffractions indicate a columnar hexagonal phase. d-Spacings are shown. Intermediate-angle XRD pattern (IAXS) at 200 °C is shown in the inset. Diffraction indexes, fiber axis, and lattice parameters are indicated.

one another to form the column (Fig. S6c, d) and the columns will arrange themselves in a hexagonal array (Fig. S6e). SAXS (Fig. 7b) at 190 °C indicate that the phase is A15 phase. The lattice parameters are determined to be $a = b = c = 73.2$ Å. Measured d-spacings at 125 °C are $d_{200} = 51.2$ Å, $d_{210} = 36.5$ Å, $d_{211} = 32.7$ Å, $d_{310} = 29.9$ Å, and $d_{222} = 26.0$ Å (Table 2). From the known molecular weight (M_{wt}) 12,202 g.mol^{-1}, we calculate an average number of dendrimers forming a sphere of the A15 phase. This value is seven molecules (6.7 ~ 7) in a sphere of the A15 lattice. The sphere diameter is 45.4 Å for the A15 phase [$D_{sph} = 2(3a^3/(32\pi)^{1/3}$] (Table 2). The models of the sphere which form the A15 lattice is shown in Fig. S6f, g. The sphere is formed by six molecules. The CTTV cores of the six molecules placed in a similar way as in the columns of the hexagonal phase. But the phenyl rings and the alkyl groups are highly disordered to form a sphere. Fig. S6f and S6g represent the top view and the side view respectively. A schematic representation of the A15 lattice is provided in Fig. S6h.

The mechanism of formation of the spheres in case of the A15 phase of **(4-3,4-3,5)12G2-CTTV** is shown in Fig. 8. It can be noticed that the seven CTTV dendrimers are stacked on one another in a similar way as in the Φ_h phase but their outer side phenyl rings and the alkyl chains are flexibly distorted to take a spherical shape for the formation of the QLC phase. The mechanism of formation of spheres for QLC phase in case of **(3,4,5)12G-CTTV** or for A15 phase of **(4-3,4,5)12G-CTTV** are similar.

Fig. 9 illustrates the oriented fiber of **(3,4)dm8*G1-CTTV** together with the helical model of its chiral column, which was published previously [73].

DSC traces (Fig. 2, Table S1) indicate that **(4-3,4)dm8*G1-CTTV** exhibits three distinguished phases. Below 148 °C, there is a Φ_h^{io} phase (Φ_h^{io1}). From 148 to 182 ° C, a center rectangular crystalline columnar ($\Phi_{r\text{-}c}^{io}$) phase with intracolumnar order is found. From 182 °C to the melting point 217 °C there is another Φ_h^{io} phase (Φ_h^{io2}). IAXS for **(4-3,4)dm8*G1-CTTV** and their corresponding radial plots at 100 °C is shown in Figure 10 and have been summarized in Table 2. The lattice parameters at 100 °C (Φ_h^{io1}) are determined to be $a = 43.0$ and $b = 43.0$ Å. Measured d-spacings at 25 °C are $d_{100} = 37.3$ Å, $d_{110} = 21.1$ Å, and $d_{200} = 18.6$ Å (Table 2). The lattice parameters at 160 °C ($\Phi_{r\text{-}c}^{io}$) are determined to be $a = 70.4$ Å and $b = 43.0$ Å. Measured d-spacings are $d_{110} = 38.6$ Å, $d_{020} = 35.2$ Å, $d_{200} = 23.0$ Å, $d_{130} = 20.9$ Å, $d_{220} = 19.3$ Å, and $d_{040} = 17.6$ Å (Table 2). The lattice parameters at 200 °C (Φ_h^{io2}) are determined to be $a = 41.3$ and $b = 41.3$ Å. Measured d-spacings at 200 °C are $d_{100} = 35.8$ Å, $d_{110} = 20.7$ Å, and $d_{200} = 17.9$ Å (Table 2). From the known molecular weight (M_{wt}) 5407.8 g.mol^{-1}, we determine the average number of dendrimers forming the supramolecular column stratum to be one molecule ($\mu = 0.9 \sim 1$ for Φ_h^{io1} and Φ_h^{io2}). The column diameter is 43.0 Å for Φ_h^{io1} phase while the column diameter for the Φ_h^{io2} phase is 41.3 Å [$D_{col} = a$]. For the $\Phi_{r\text{-}c}^{io}$ phase, there are two molecules ($\mu = 1.8 \sim 2$) for $\Phi_{r\text{-}c}^{io}$ phase per stratum. The *c*-axis of this monoclinic phase is along the fiber axis. Figure S7 consists of the molecular models for Φ_h^{io1}, $\Phi_{r\text{-}c}^{io}$, and Φ_h^{io2} phases. For Φ_h^{io1} and Φ_h^{io2} the repeat unit is formed by one molecule (Fig. S7a–c). For the Φ_h^{io} phases, in the first step, one molecule is placed with highly distorted CTTV core (Fig. S7a–c). In the second step, another molecule is placed on top of the first molecule at 4.9 Å (Fig. S7e–g). Thus, each molecule will stack over one another to form the column (Fig. S7f and S7h) and the columns will arrange in a hexagonal array (Fig. S7h). For $\Phi_{r\text{-}c}^{io}$ phase, the repeat unit is formed by two molecules (Fig. S7d). For the $\Phi_{r\text{-}c}^{io}$ phase, in the first step, two molecules are placed in front of each other with distorted CTTV core (Figure S7d) to form an oval shape repeat unit. In the second step, another dimer is placed on top of the first dimer at 4.9 Å. Thus, these dimers will stack over one another to form the column of the center rectangular phase ($\Phi_{r\text{-}c}^{io}$) (Fig. S7g) and thus these columns will arrange themselves in a center rectangular array (Fig. S7i).

Conclusions

The primary-tertiary structure-function is one of the most fundamental concepts responsible for biological and synthetic self-organizations [39,42,43,84,85]. The less understood part of this concept refers to the role of the conformational flexibility during this process. In this publication we compare the dynamics of an *n*-alkylated with dendronized conformationally flexible CTTV with its less flexible CTV, Tp and THB. These experiments demonstrated that conformational flexibility may select unusual equilibrium structures while more rigid structures may freeze non-equilibrium structures since more rigid apex molecules increase phase transition temperatures while decreasing the dynamics of the self-organized system. Helical columnar structures generated from chiral spheres and from crowns, QLC and Frank-Kasper A15 phases dominate the hierarchical self-organizations observed so far with dendronized CTTV. However, the structural requirements that mediate the transition from a supramolecular column to supramolecular spheres or elongated columns and their accompanied self-organizations require additional experiments in order to be elucidated. Additional experiments are required to explain how conformational flexibility changes the mechanism of self-organization of supramolecular spheres in different Frank-Kasper and quasicrystal phases. The concept raised in this report could inspire additional discoveries in other forms of

self-organized soft matter including lipids, block co-polymers, surfactants, dendron-like silsesquioxane-cage molecules, [93–125], which were reported to forms complex architectures including Frank-Kasper phases (Fig. 10).

Declaration of Competing Interest

The authors declare that they have no known competing financial interests or personal relationships that could have appeared to influence the work reported in this paper.

Acknowledgment

Financial support by the National Science Foundation (DMR-1807127, DMR-1720530, and DMR- 2104554), the Humboldt Foundation, and the P. Roy Vagelos Chair at Penn (all to V.P.) is gratefully acknowledged. B.E.P. thanks the Howard Hughes Medical Institute for an International Student Research Fellowship.

Supplementary materials

Supplementary material associated with this article can be found, in the online version, at doi:10.1016/j.giant.2022.100096.

References

[1] V. Percec, M. Peterca, A.E. Dulcey, M.R. Imam, S.D. Hudson, S. Nummelin, P. Adelman, P.A. Heiney, Hollow spherical supramolecular dendrimers, J. Am. Chem. Soc. 130 (2008) 13079–13094, https://doi.org/10.1021/ja8034703.

[2] V. Percec, J. Smidrkal, M. Peterca, C.M. Mitchell, S. Nummelin, A.E. Dulcey, M. J. Sienkowska, P.A. Heiney, Self-assembly of hybrid dendrons with complex primary structure into functional helical pores, Chem. A Eur. J. 13 (2007) 3989–4007, https://doi.org/10.1002/chem.200601582.

[3] V. Percec, P. Chu, G. Ungar, J. Zhou, Rational design of the first nonspherical dendrimer which displays calamitic nematic and smectic thermotropic liquid crystalline phases, J. Am. Chem. Soc. 117 (1995) 11441–11454, https://doi.org/10.1021/ja00151a008.

[4] K. Kanie, M. Matsubara, X. Zeng, F. Liu, G. Ungar, H. Nakamura, A. Muramatsu, Simple cubic packing of gold nanoparticles through rational design of their dendrimeric corona, J. Am. Chem. Soc. 134 (2012) 808–811, https://doi.org/10.1021/ja2095816.

[5] V. Percec, M. Peterca, Y. Tsuda, B.M. Rosen, S. Uchida, M.R. Imam, G. Ungar, P. A. Heiney, Elucidating the structure of the Pm3n cubic phase of supramolecular dendrimers through the modification of their aliphatic to aromatic volume ratio, Chem. Eur. J. 15 (2009) 8994–9004, https://doi.org/10.1002/chem.200901324.

[6] V. Percec, J.G. Rudick, M. Peterca, M.E. Yurchenko, J. Smidrkal, P.A. Heiney, Supramolecular structural diversity among first-generation hybrid dendrimers and twin dendrons, Chem. Eur. J. 14 (2008) 3355–3362, https://doi.org/10.1002/chem.200701658.

[7] V. Percec, B.C. Won, M. Peterca, P.A. Heiney, Expanding the structural diversity of self-assembling dendrons and supramolecular dendrimers via complex building blocks, J. Am. Chem. Soc. 129 (2007) 11265–11278, https://doi.org/10.1021/ja073714j.

[8] V. Percec, M. Peterca, M.J. Sienkowska, M.A. Ilies, E. Aqad, J. Smidrkal, P. A. Heiney, Synthesis and retrostructural analysis of libraries of AB_3 and constitutional isomeric AB_2 phenylpropyl ether-based supramolecular dendrimers, J. Am. Chem. Soc. 128 (2006) 3324–3334, https://doi.org/10.1021/ja060062a.

[9] V. Percec, M.N. Holerca, S. Nummelin, J.J. Morrison, M. Glodde, J. Smidrkal, M. Peterca, B.M. Rosen, S. Uchida, V.S.K. Balagurusamy, M.J. Sienkowska, P. A. Heiney, Exploring and expanding the structural diversity of self-assembling dendrons through combinations of AB, constitutional isomeric AB_2, and AB_3 biphenyl-4-methyl ether building blocks, Chem. Eur. J. 12 (2006) 6216–6241, https://doi.org/10.1002/chem.200600178.

[10] V. Percec, C.M. Mitchell, W.D. Cho, S. Uchida, M. Glodde, G. Ungar, X. Zeng, Y. Liu, V.S.K. Balagurusamy, P.A. Heiney, Designing libraries of first generation AB_3 and AB_2 self-assembling dendrons *via* the primary structure generated from combinations of $(AB)_y$–AB_3 and $(AB)_y$–AB_2 building blocks, J. Am. Chem. Soc. 126 (2004) 6078–6094, https://doi.org/10.1021/ja049846j.

[11] G. Ungar, Y. Liu, X. Zeng, V. Percec, W.D. Cho, Giant supramolecular liquid crystal lattice, Science 299 (2003) 1208–1211, https://doi.org/10.1126/science.1078849.

[12] X. Zeng, G. Ungar, Y. Liu, V. Percec, A.E. Dulcey, J.K. Hobbs, Supramolecular dendritic liquid quasicrystals, Nature 428 (2004) 157–160, https://doi.org/10.1038/nature02368.

[13] G. Ungar, D. Abramic, V. Percec, J.A. Heck, Self-assembly of twin tapered bisamides into supramolecular columns exhibiting hexagonal columnar mesophases. Structural evidence for a microsegregated model of the supramolecular column, Liq. Cryst. 21 (1996) 73–86, https://doi.org/10.1080/02678299608033797.

[14] D.R. Dukeson, G. Ungar, V.S.K. Balagurusamy, V. Percec, G.A. Johansson, M. Glodde, Application of isomorphous replacement in the structure determination of a cubic liquid crystal phase and location of counterions, J. Am. Chem. Soc. 125 (2003) 15974–15980, https://doi.org/10.1021/ja037380j.

[15] V. Percec, W.D. Cho, G. Ungar, D.J.P. Yeardley, Synthesis and NaOTf mediated self-assembly of monodendritic crown ethers, Chem. Eur. J. 8 (2002) 2011–2025, https://doi.org/10.1002/1521-3765(20020503)8:9.2011::AID-CHEM2011.3.0.CO;2-3.

[16] V. Percec, M.N. Holerca, S. Uchida, W.D. Cho, G. Ungar, Y. Lee, D.J.P. Yeardley, Exploring and expanding the three-dimensional structural diversity of supramolecular dendrimers with the aid of libraries of alkali metals of their AB_3 minidendritic carboxylates, Chem. Eur. J. 8 (2002) 1106–1117, https://doi.org/10.1002/1521-3765(20020301)8:5.1106::AID-CHEM1106.3.0.CO;2-G.

[17] V. Percec, W.D. Cho, G. Ungar, D.J.P. Yeardley, Synthesis and structural analysis of two constitutional isomeric libraries of AB_2-based monodendrons and supramolecular dendrimers, J. Am. Chem. Soc. 123 (2001) 1302–1315, https://doi.org/10.1021/ja0037771.

[18] G. Ungar, V. Percec, M.N. Holerca, G. Johansson, J.A. Heck, Heat-shrinking spherical and columnar supramolecular dendrimers: their interconversion and dependence of their shape on molecular taper angle, Chem. Eur. J. 6 (2000) 1258–1266, https://doi.org/10.1002/(SICI)1521-3765(20000403)6:7.1258::AID-CHEM1258.3.0.CO;2-O.

[19] V. Percec, W.D. Cho, G. Ungar, D.J.P. Yeardley, From molecular flat tapers, discs, and cones to supramolecular cylinders and spheres using Fréchet-type monodendrons modified on their leriphery, Angew. Chem. Int. Ed. 39 (2000) 1597–1602, https://doi.org/10.1002/(SICI)1521-3773(20000502)39:9.1597::AID-ANIE1597.3.0.CO;2-I.

[20] V. Percec, W.D. Cho, M. Möller, S.A. Prokhorova, G. Ungar, D.J.P. Yeardley, Design and structural analysis of the first spherical monodendron self-organizable in a cubic lattice, J. Am. Chem. Soc. 122 (2000) 4249–4250, https://doi.org/10.1021/ja9943400.

[21] V. Percec, W.D. Cho, G. Ungar, Increasing the diameter of cylindrical and spherical supramolecular dendrimers by decreasing the solid angle of their monodendrons *via* periphery functionalization, J. Am. Chem. Soc. 122 (2000) 10273–10281, https://doi.org/10.1021/ja0024643.

[22] V. Percec, W.D. Cho, P.E. Mosier, G. Ungar, D.J.P. Yeardley, Structural analysis of cylindrical and spherical supramolecular dendrimers quantifies the concept of monodendron shape control by generation number, J. Am. Chem. Soc. 120 (1998) 11061–11070, https://doi.org/10.1021/ja9819007.

[23] V. Percec, A.E. Dulcey, M. Peterca, M. Ilies, S. Nummelin, M.J. Sienkowska, P. A. Heiney, Principles of self-assembly of helical pores from dendritic dipeptides, Proc. Natl. Acad. Sci. U.S.A. 103 (2006) 2518–2523, https://doi.org/10.1073/pnas.0509676103.

[24] V. Percec, A.E. Dulcey, V.S.K. Balagurusamy, Y. Miura, J. Smidrkal, M. Peterca, S. Nummelin, U. Edlund, S.D. Hudson, P.A. Heiney, H. Duan, S.N. Magonov, S. A. Vinogradov, Self-assembly of amphiphilic dendritic dipeptides into helical pores, Nature 430 (2004) 764–768, https://doi.org/10.1038/nature02770.

[25] V.S.K. Balagurusamy, G. Ungar, V. Percec, G. Johansson, Rational design of the first spherical supramolecular dendrimers self-organized in a novel thermotropic cubic liquid-crystalline phase and the determination of their shape by X-ray analysis, J. Am. Chem. Soc. 119 (1997) 1539–1555, https://doi.org/10.1021/ja963295i.

[26] V. Percec, C.H. Ahn, G. Ungar, D.J.P. Yeardley, M. Möller, S.S. Sheiko, Controlling polymer shape through the self-assembly of dendritic side-groups, Nature 391 (1998) 161–164, https://doi.org/10.1038/34384.

[27] S.D. Hudson, H.T. Jung, V. Percec, W.D. Cho, G. Johansson, G. Ungar, V.S. K. Balagurusamy, Direct visualization of individual cylindrical and spherical supramolecular dendrimers, Science 278 (1997) 449–452, https://doi.org/10.1126/science.278.5337.449.

[28] V. Percec, G. Johansson, G. Ungar, J. Zhou, Fluorophobic effect induces the self-assembly of semifluorinated tapered monodendrons containing crown ethers into supramolecular columnar dendrimers which exhibit a homeotropic hexagonal columnar liquid crystalline phase, J. Am. Chem. Soc. 118 (1996) 9855–9866, https://doi.org/10.1021/ja9615738.

[29] B.M. Rosen, D.A. Wilson, C.J. Wilson, M. Peterca, B.C. Won, C. Huang, L.R. Lipski, X. Zeng, G. Ungar, P.A. Heiney, V. Percec, Predicting the structure of supramolecular dendrimers via the analysis of libraries of AB_3 and constitutional isomeric AB_2 biphenylpropyl ether self-assembling dendrons, J. Am. Chem. Soc. 131 (2009) 17500–17521, https://doi.org/10.1021/ja907882n.

[30] B.M. Rosen, M. Peterca, C. Huang, X. Zeng, G. Ungar, V. Percec, Deconstruction as a strategy for the design of libraries of self-assembling dendrons, Angew. Chem. Int. Ed. 49 (2010) 7002–7005, https://doi.org/10.1002/anie.201002514.

[31] M. Peterca, M.R. Imam, P. Leowanawat, B.M. Rosen, D.A. Wilson, C.J. Wilson, X. Zeng, G. Ungar, P.A. Heiney, V. Percec, Self-assembly of hybrid dendrons into doubly segregated supramolecular polyhedral columns and vesicles, J. Am. Chem. Soc. 132 (2010) 11288–11305, https://doi.org/10.1021/ja104432d.

[32] A. Rapp, I. Schnell, D. Sebastiani, S.P. Brown, V. Percec, H.W. Spiess, Supramolecular assembly of dendritic polymers elucidated by ^{1}H and ^{13}C solid-state MAS NMR spectroscopy, J. Am. Chem. Soc. 125 (2003) 13284–13297, https://doi.org/10.1021/ja035127d.

[33] V. Percec, M.R. Imam, M. Peterca, D.A. Wilson, P.A. Heiney, Self-assembly of dendritic crowns into chiral supramolecular spheres, J. Am. Chem. Soc. 131 (2009) 1294–1304, https://doi.org/10.1021/ja8087778.

[34] V. Percec, M.R. Imam, M. Peterca, D.A. Wilson, R. Graf, H.W. Spiess, V.S. K. Balagurusamy, P.A. Heiney, Self-assembly of dendronized triphenylenes into helical pyramidal columns and chiral spheres, J. Am. Chem. Soc. 131 (2009) 7662–7677, https://doi.org/10.1021/ja8094944.

[35] V. Percec, S. Wang, N. Huang, B.E. Partridge, X. Wang, D. Sahoo, D.J. Hoffman, J. Malineni, M. Peterca, R.L. Jezorek, N. Zhang, H. Daud, P.D. Sung, E. R. McClure, S.L. Song, An accelerated modular-orthogonal Ni-catalyzed methodology to symmetric and nonsymmetric constitutional isomeric AB_2 to AB_9 dendrons exhibiting unprecedented self-organizing principles, J. Am. Chem. Soc. 143 (2021) 17724–17743, https://doi.org/10.1021/jacs.1c08502.

[36] V. Percec, C.H. Ahn, T.K. Bera, G. Ungar, D.J.P. Yeardley, Coassembly of a hexagonal columnar liquid crystalline superlattice from polymer(s) coated with a three-cylindrical bundle supramolecular dendrimer, Chem. Eur. J. 5 (1999) 1070–1083, https://doi.org/10.1002/(SICI)1521-3765(19990301)5:3.1070::AID-CHEM1070.3.0.CO;2-9.

[37] V. Percec, T.K. Bera, M. Glodde, Q. Fu, V.S.K. Balagurusamy, P.A. Heiney, Hierarchical self-assembly, coassembly, and self-organization of novel liquid crystalline lattices and superlattices from a twin-tapered dendritic benzamide and its four-cylinder-bundle supramolecular polymer, Chem. Eur. J. 9 (2003) 921–935, https://doi.org/10.1002/chem.200390114.

[38] V. Percec, M.R. Imam, M. Peterca, P. Leowanawat, Self-organizable vesicular columns assembled from polymers dendronized with semifluorinated Janus dendrimers act as reverse thermal actuators, J. Am. Chem. Soc. 134 (2012) 4408–4420, https://doi.org/10.1021/ja2118267.

[39] B.M. Rosen, C.J. Wilson, D.A. Wilson, M. Peterca, M.R. Imam, V. Percec, Dendron-mediated self-assembly, disassembly, and self-organization of complex systems, Chem. Rev. 109 (2009) 6275–6540, https://doi.org/10.1021/cr900157q.

[40] V. Percec, M.R. Imam, T.K. Bera, V.S.K. Balagurusamy, M. Peterca, P.A. Heiney, Self-assembly of semifluorinated janus-dendritic benzamides into bilayered pyramidal columns, Angew. Chem. Int. Ed. 44 (2005) 4739–4745, https://doi.org/10.1002/anie.200501254.

[41] V. Percec, G. Ungar, M. Peterca, Self-assembly in action, Science (2006), https://doi.org/10.1126/science.1129512.

[42] H.J. Sun, S. Zhang, V. Percec, From structure to function *via* complex supramolecular dendrimer systems, Chem. Soc. Rev. 44 (2015) 3900–3923, https://doi.org/10.1039/C4CS00249K.

[43] J.G. Rudick, V. Percec, Induced helical backbone conformations of self-organizable dendronized polymers, Acc. Chem. Res. 41 (2008) 1641–1652, https://doi.org/10.1021/ar800086w.

[44] J.G. Rudick, V. Percec, Helical chirality in dendronized polyarylacetylenes, New J. Chem. 31 (2007) 1083–1096, https://doi.org/10.1039/B616449H.

[45] V. Percec, C.H. Ahn, W.D. Cho, A.M. Jamieson, J. Kim, T. Leman, M. Schmidt, M. Gerle, M. Möller, S.A. Prokhorova, S.S. Sheiko, S.Z.D. Cheng, A. Zhang, G. Ungar, D.J.P. Yeardley, Visualizable cylindrical macromolecules with controlled stiffness from backbones containing libraries of self-assembling dendritic side groups, J. Am. Chem. Soc. 120 (1998) 8619–8631, https://doi.org/10.1021/ja981211v.

[46] V. Percec, M. Glodde, T.K. Bera, Y. Miura, I. Shiyanovskaya, K.D. Singer, V.S. K. Balagurusamy, P.A. Heiney, I. Schnell, A. Rapp, H.W. Spiess, S.D. Hudson, H. Duan, Self-organization of supramolecular helical dendrimers into complex electronic materials, Nature 419 (2002) 384–387, https://doi.org/10.1038/nature01072.

[47] V. Percec, G. Johansson, J. Heck, G. Ungarb, S.V. Battyb, Molecular recognition directed self-assembly of supramolecular cylindrical channel-like architectures from 6,7,9,10,12,13,15,16-octahydro-1,4,7,10,13-pentaoxabenzocyclopentadecen-2-ylmethyl 3,4,5-tris(p-dodecyloxybenzyloxy)benzoate, J. Chem. Soc. Perkin Trans. 1 (1993) 1411–1420, https://doi.org/10.1039/P19930001411.

[48] V. Percec, J.G. Rudick, M. Peterca, M. Wagner, M. Obata, C.M. Mitchell, W. D. Cho, V.S.K. Balagurusamy, P.A. Heiney, Thermoreversible cis−cisoidal to cis−transoidal isomerization of helical dendronized polyphenylacetylenes, J. Am. Chem. Soc. 127 (2005) 15257–15264, https://doi.org/10.1021/ja055406w.

[49] V. Percec, J. Heck, D. Tomazos, F. Falkenberg, H. Blackwell, G. Ungar, Self-assembly of taper-shaped monoesters of oligo(ethylene oxide) with 3,4,5-tris(p-dodecyloxybenzyloxy)benzoic acid and of their polymethacrylates into tubular supramolecular architectures displaying a columnar mesophase, J. Chem. Soc. Perkin Trans. 1 (1993) 2799–2811, https://doi.org/10.1039/P19930002799.

[50] G. Johansson, V. Percec, G. Ungar, D. Abramic, Molecular recognition directed self-assembly of tubular liquid crystalline and crystalline supramolecular architectures from taper shaped (15-crown-5)methyl 3,4,5-tris(p-alkyloxybenzyloxy)benzoates and (15-crown-5)methyl 3,4,5-tris(p-dodecyloxy)benzoate, J. Chem. Soc. Perkin Trans. 1 (1994) 447–459, https://doi.org/10.1039/P19940000447.

[51] V. Percec, D. Tomazos, J. Heck, H. Blackwell, G. Ungar, Self-assembly of taper-shaped monoesters of oligo(ethylene oxide) with 3,4,5-tris(n-dodecan-1-yloxy) benzoic acid and of their polymethacrylates into tubular supramolecular architectures displaying a columnar hexagonal mesophase, J. Chem. Soc. Perkin Trans. 2 (1994) 31–44, https://doi.org/10.1039/P29940000031.

[52] V. Percec, D. Schlueter, J.C. Ronda, G. Johansson, G. Ungar, J.P. Zhou, Tubular architectures from polymers with tapered side groups. Assembly of side groups *via* a rigid helical chain conformation and flexible helical chain conformation induced via assembly of side groups, Macromolecules 29 (1996) 1464–1472, https://doi.org/10.1021/ma951244k.

[53] Y.K. Kwon, S.N. Chvalun, J. Blackwell, V. Percec, J.A. Heck, Effect of Temperature on the supramolecular tubular structure in oriented fibers of a poly (methacrylate) with tapered side groups, Macromolecules 28 (1995) 1552–1558, https://doi.org/10.1021/ma00109a029.

[54] V. Percec, D. Schlueter, Mechanistic investigations on the formation of supramolecular cylindrical shaped oligomers and polymers by living ring opening metathesis polymerization of a 7-oxanorbornene monomer substituted with two tapered monodendrons, Macromolecules 30 (1997) 5783–5790, https://doi.org/10.1021/ma970157k.

[55] V. Percec, D. Schlueter, G. Ungar, S.Z.D. Cheng, A. Zhang, Hierarchical control of internal superstructure, diameter, and stability of supramolecular and macromolecular columns generated from tapered monodendritic building blocks, Macromolecules 31 (1998) 1745–1762, https://doi.org/10.1021/ma971459p.

[56] V. Percec, J.A. Heck, D. Tomazos, G. Ungar, The influence of the complexation of sodium and lithium triflate on the self-assembly of tubular-supramolecular architectures displaying a columnar mesophase based on taper-shaped monoesters of oligoethylene oxide with 3,4,5-tris[*p*-(*n-dodecan*-1-*yloxy*) *benzyloxy*]benzoic acid and of their polymethacrylates, J. Chem. Soc. Perkin Trans. 2 (1993) 2381–2388, https://doi.org/10.1039/P29930002381.

[57] M. Peterca, V. Percec, M.R. Imam, P. Leowanawat, K. Morimitsu, P.A. Heiney, Molecular structure of helical supramolecular dendrimers, J. Am. Chem. Soc. 130 (2008) 14840–14852, https://doi.org/10.1021/ja806524m.

[58] C. Roche, H.J. Sun, M.E. Prendergast, P. Leowanawat, B.E. Partridge, P.A. Heiney, F. Araoka, R. Graf, H.W. Spiess, X. Zeng, G. Ungar, V. Percec, Homochiral columns constructed by chiral self-sorting during supramolecular helical organization of hat-ahaped molecules, J. Am. Chem. Soc. 136 (2014) 7169–7185, https://doi.org/10.1021/ja5035107.

[59] C. Roche, H.J. Sun, P. Leowanawat, F. Araoka, B.E. Partridge, M. Peterca, D. A. Wilson, M.E. Prendergast, P.A. Heiney, R. Graf, H.W. Spiess, X. Zeng, G. Ungar, V. Percec, A supramolecular helix that disregards chirality, Nat. Chem. 8 (2016) 80–89, https://doi.org/10.1038/nchem.2397.

[60] B.E. Partridge, L. Wang, D. Sahoo, J.T. Olsen, P. Leowanawat, C. Roche, H. Ferreira, K.J. Reilly, X. Zeng, G. Ungar, P.A. Heiney, R. Graf, H.W. Spiess, V. Percec, Sequence-defined dendrons dictate supramolecular cogwheel assembly of dendronized perylene bisimides, J. Am. Chem. Soc. 141 (2019) 15761–15766, https://doi.org/10.1021/jacs.9b08714.

[61] L. Wang, B.E. Partridge, N. Huang, J.T. Olsen, D. Sahoo, X. Zeng, G. Ungar, R. Graf, H.W. Spiess, V. Percec, Extraordinary acceleration of cogwheel helical self-organization of dendronized perylene bisimides by the dendron sequence encoding their tertiary structure, J. Am. Chem. Soc. 142 (2020) 9525–9536, https://doi.org/10.1021/jacs.0c03353.

[62] M.N. Holerca, D. Sahoo, M. Peterca, B.E. Partridge, P.A. Heiney, V. Percec, A tetragonal phase self-organized from unimolecular spheres assembled from a substituted poly(2-oxazoline), Macromolecules 50 (2017) 375–385, https://doi.org/10.1021/acs.macromol.6b02298.

[63] M.N. Holerca, D. Sahoo, B.E. Partridge, M. Peterca, X. Zeng, G. Ungar, V. Percec, Dendronized poly(2-oxazoline) displays within only five monomer repeat units liquid quasicrystal, A15 and σ Frank–Kasper phases, J. Am. Chem. Soc. 140 (2018) 16941–16947, https://doi.org/10.1021/jacs.8b11103.

[64] M.N. Holerca, M. Peterca, B.E. Partridge, Q. Xiao, G. Lligadas, M.J. Monteiro, V. Percec, Monodisperse macromolecules by self-interrupted living polymerization, J. Am. Chem. Soc. 142 (2020) 15265–15270, https://doi.org/10.1021/jacs.0c07912.

[65] V. Percec, J. Heck, M. Lee, G. Ungar, A. Alvarez-Castillo, Poly{2-vinyloxyethyl 3,4,5-tris[4-(*n-dodecanyloxy*)*benzyloxy*]benzoate}: a self-assembled supramolecular polymer similar to tobacco mosaic virus, J. Mater. Chem. 2 (1992) 1033–1039, https://doi.org/10.1039/JM9920201033.

[66] V. Percec, M. Lee, Molecular engineering of liquid crystal polymers by living polymerization. XXIII. Synthesis and characterization of AB block copolymers based on ω-[(4-*cyano*-4′-*biphenyl*)-*oxy*]alkyl vinyl ether, 1H, 1H, 2H, 2H-perfluorodecyl vinyl ether, and 2-(4-biphenyloxy)ethyl vinyl ether with 1H, 1H, 2H, 2H-perfluorodecyl vinyl ether, J. Macromol. Sci. Part A 29 (1992) 723–740, https://doi.org/10.1080/10601329208054112.

[67] G. Johansson, V. Percec, G. Ungar, K. Smith, Fluorophobic effect generates a systematic approach to the synthesis of the simplest class of rodlike liquid crystals containing a single benzene unit, Chem. Mater. 9 (1997) 164–175, https://doi.org/10.1021/cm960267q.

[68] H.S. Creel, M.J. Fournier, T.L. Mason, D.A. Tirrell, Genetically directed syntheses of new polymeric materials: efficient expression of a monodisperse copolypeptide containing fourteen tandemly repeated -(AlaGly)4ProGluGly- elements, Macromolecules 24 (1991) 1213–1214, https://doi.org/10.1021/ma00005a040.

[69] K.P. McGrath, M.J. Fournier, T.L. Mason, D.A. Tirrell, Genetically directed syntheses of new polymeric materials. Expression of artificial genes encoding proteins with repeating -(AlaGly)3ProGluGly- elements, J. Am. Chem. Soc. 114 (1992) 727–733, https://doi.org/10.1021/ja00028a048.

[70] V. Percec, M.N. Holerca, S.N. Magonov, D.J.P. Yeardley, G. Ungar, H. Duan, S. D. Hudson, Poly(oxazolines)s with tapered minidendritic side groups. The simplest cylindrical models to investigate the formation of two-dimensional and three-dimensional order by direct visualization, Biomacromolecules 2 (2001) 706–728, https://doi.org/10.1021/bm015550j.

[71] V. Percec, M.N. Holerca, S. Uchida, D.J.P. Yeardley, G. Ungar, Poly(oxazoline)s with tapered minidendritic side groups as models for the design of synthetic macromolecules with tertiary structure. A demonstration of the limitations of living polymerization in the design of 3-D structures based on single polymer chains, Biomacromolecules 2 (2001) 729–740, https://doi.org/10.1021/bm015559l.

[72] V. Percec, M.N. Holerca, Detecting the shape change of complex macromolecules during their synthesis with the aid of kinetics. A new lesson from biology, Biomacromolecules 1 (2000) 6–16, https://doi.org/10.1021/bm005507g.

[73] D. Sahoo, M.R. Imam, M. Peterca, B.E. Partridge, D.A. Wilson, X. Zeng, G. Ungar, P.A. Heiney, V. Percec, Hierarchical self-organization of chiral columns from chiral supramolecular spheres, J. Am. Chem. Soc. 140 (2018) 13478–13487, https://doi.org/10.1021/jacs.8b09174.

[74] M. Peterca, M.R. Imam, S.D. Hudson, B.E. Partridge, D. Sahoo, P.A. Heiney, M. L. Klein, V. Percec, Complex arrangement of orthogonal nanoscale columns via a supramolecular orientational memory effect, ACS Nano 10 (2016) 10480–10488, https://doi.org/10.1021/acsnano.6b06419.

[75] D. Sahoo, M. Peterca, E. Aqad, B.E. Partridge, P.A. Heiney, R. Graf, H.W. Spiess, X. Zeng, V. Percec, Tetrahedral arrangements of perylene bisimide columns via supramolecular orientational memory, ACS Nano 11 (2017) 983–991, https://doi.org/10.1021/acsnano.6b07599.

[76] D. Sahoo, M. Peterca, E. Aqad, B.E. Partridge, M.L. Klein, V. Percec, Losing supramolecular orientational memory via self-organization of a misfolded secondary structure, Polym. Chem. 9 (2018) 2370–2381, https://doi.org/10.1039/C8PY00187A.

[77] N. Huang, M.R. Imam, M.J. Sienkowska, M. Peterca, M.N. Holerca, D.A. Wilson, B.M. Rosen, B.E. Partridge, Q. Xiao, V. Percec, Supramolecular spheres assembled from covalent and supramolecular dendritic crowns dictate the supramolecular orientational memory effect mediated by Frank-Kasper phases, Giant 1 (2020), 100001, https://doi.org/10.1016/j.giant.2020.100001.

[78] N. Huang, Q. Xiao, M. Peterca, X. Zeng, V. Percec, Self-Organisation of rhombitruncated cuboctahedral hexagonal columns from an amphiphilic Janus dendrimer, Mol. Phys. 119 (2021), e1902586, https://doi.org/10.1080/00268976.2021.1902586.

[79] V. Percec, N. Huang, Q. Xiao, B.E. Partridge, D. Sahoo, M.R. Imam, M. Peterca, R. Graf, H.-.W. Spiess, X. Zeng, G. Ungar, Self-organization of rectangular bipyramidal helical columns by supramolecular orientational memory epitaxially nucleated from a Frank-Kasper σ phase, Giant 9 (2022), 100084, https://doi.org/10.1016/j.giant.2021.100084.

[80] V. Percec, C.G. Cho, C. Pugh, Cyclotrimerization versus cyclotetramerization in the electrophilic oligomerization of 3,4-bis(methyloxy)benzyl derivatives, Macromolecules 24 (1991) 3227–3234, https://doi.org/10.1021/ma00011a029.

[81] V. Percec, C.G. Cho, C. Pugh, D. Tomazos, Synthesis and characterization of branched liquid-crystalline polyethers containing cyclotetraveratrylene-based disk-like mesogens, Macromolecules 25 (1992) 1164–1176, https://doi.org/10.1021/ma00029a025.

[82] V. Percec, C.G. Cho, C. Pugh, Alkyloxy-substituted CTTV derivatives that exhibit columnar mesophases, J. Mater. Chem. 1 (1991) 217–222, https://doi.org/10.1039/JM9910100217.

[83] P.A. Heiney, Datasqueeze: a software tool for powder and small-angle X-ray diffraction analysis, Comm. Powder Diffr. Newsl. 32 (2005) 9–11.

[84] M.S. Kaucher, M. Peterca, A.E. Dulcey, A.J. Kim, S.A. Vinogradov, D.A. Hammer, P.A. Heiney, V. Percec, Selective transport of water mediated by porous dendritic dipeptides, J. Am. Chem. Soc. 129 (2007) 11698–11699, https://doi.org/10.1021/ja076066c.

[85] V. Percec, J.G. Rudick, M. Peterca, P.A. Heiney, Nanomechanical function from self-organizable dendronized helical polyphenylacetylenes, J. Am. Chem. Soc. 130 (2008) 7503–7508, https://doi.org/10.1021/ja801863e.

[86] B.M. Rosen, C. Roche, V. Percec, Self-assembly of dendritic dipeptides as a model of chiral selection in primitive biological systems, Top. Curr. Chem. 333 (2013) 213–253, https://doi.org/10.1007/128_2012_398.

[87] V. Percec, A.E. Dulcey, M. Peterca, P. Adelman, R. Samant, V.S.K. Balagurusamy, P.A. Heiney, Helical pores self-assembled from homochiral dendritic dipeptides based on L-Tyr and nonpolar alpha-amino acids, J. Am. Chem. Soc. 129 (2007) 5992–6002, https://doi.org/10.1021/ja071088k.

[88] V. Percec, A.E. Dulcey, M. Peterca, M. Ilies, M.J. Sienkowska, P.A. Heiney, Programming the internal structure and stability of helical pores self-assembled from dendritic dipeptides via the protective groups of the peptide, J. Am. Chem. Soc. 127 (2005) 17902–17909, https://doi.org/10.1021/ja056313h.

[89] M. Peterca, V. Percec, A.E. Dulcey, S. Nummelin, S. Korey, M. Ilies, P.A. Heiney, Self-assembly, structural, and retrostructural analysis of dendritic dipeptide pores undergoing reversible circular to elliptical shape change, J. Am. Chem. Soc. 128 (2006) 6713–6720, https://doi.org/10.1021/ja0611902.

[90] B.M. Rosen, M. Peterca, K. Morimitsu, A.E. Dulcey, P. Leowanawat, A.-.M. Resmerita, M.R. Imam, V. Percec, Programming the supramolecular helical polymerization of dendritic dipeptides via the stereochemical information of the dipeptide, J. Am. Chem. Soc. 133 (2011) 5135–5151, https://doi.org/10.1021/ja200280h.

[91] V. Percec, M. Glodde, M. Peterca, A. Rapp, I. Schnell, H.W. Spiess, T.K. Bera, Y. Miura, V.S.K. Balagurusamy, E. Aqad, P.A. Heiney, Self-assembly of semifluorinated dendrons attached to electron-donor groups mediates their π-stacking via a helical pyramidal column, Chem. Eur. J. 12 (2006) 6298–6314, https://doi.org/10.1002/chem.200501195.

[92] V. Percec, E. Aqad, M. Peterca, M.R. Imam, M. Glodde, T.K. Bera, Y. Miura, V.S. K. Balagurusamy, P.C. Ewbank, F. Würthner, P.A. Heiney, Self-assembly of semifluorinated minidendrons attached to electron-acceptor groups into pyramidal columns, Chem. Eur. J. 13 (2007) 3330–3345, https://doi.org/10.1002/chem.200600901.

[93] P. Mariani, V. Luzzati, H. Delacroix, Cubic phases of lipid-containing systems: structure analysis and biological implications, J. Mol. Biol. 204 (1988) 165–189, https://doi.org/10.1016/0022-2836(88)90607-9.

[94] R. Vargas, P. Mariani, A. Gulik, V. Luzzati, Cubic phases of lipid-containing systems: the structure of phase Q223 (space group Pm3n). An X-ray scattering study, J. Mol. Biol 225 (1992) 137–145, https://doi.org/10.1016/0022-2836(92)91031-j.

[95] J. Charvolin, J.F. Sadoc, Periodic systems of frustrated fluid films and « micellar » cubic structures in liquid crystals, J. Phys. Fr. 49 (1988) 521–526, https://doi.org/10.1051/jphys:01988004903052100.

[96] L. Paccamiccio, M. Pisani, F. Spinozzi, C. Ferrero, S. Finet, P. Mariani, Pressure effects on lipidic direct phases: the dodecyl trimethyl ammonium chloride−water system, J. Phys. Chem. B 110 (2006) 12410–12418, https://doi.org/10.1021/jp054467d.

[97] M. Bastos, T. Silva, V. Teixeira, K. Nazmi, J.G.M. Bolscher, S.S. Funari, D. Uhríková, Lactoferrin-derived antimicrobial peptide induces a micellar cubic phase in a model membrane system, Biophys. J. 101 (2011) L20–L22, https://doi.org/10.1016/j.bpj.2011.06.038.

[98] H. Delacroix, T. Gulik-Krzywicki, P. Mariani, V. Luzzati, Freeze-fracture electron microscope study of lipid systems: the cubic phase of space group Pm3n, J. Mol. Biol. 229 (1993) 526–539, https://doi.org/10.1006/jmbi.1993.1052.

[99] Y. Li, S.T. Lin, W.A. Goddard, Efficiency of various lattices from hard ball to soft ball: theoretical study of thermodynamic properties of dendrimer liquid crystal from atomistic simulation, J. Am. Chem. Soc. 126 (2004) 1872–1885, https://doi.org/10.1021/ja038617e.

[100] P. Ziherl, R.D. Kamien, Maximizing entropy by minimizing area: towards a new principle of self-organization, J. Phys. Chem. B 105 (2001) 10147–10158, https://doi.org/10.1021/jp010944q.

[101] C.R. Iacovella, A.S. Keys, S.C. Glotzer, Self-assembly of soft-matter quasicrystals and their approximants, Proc. Natl. Acad. Sci. U.S.A. 108 (2011) 20935–20940, https://doi.org/10.1073/pnas.1019763108.

[102] S. Lee, M.J. Bluemle, F.S. Bates, Discovery of a Frank-Kasper σ phase in sphere-forming block copolymer melts, Science 330 (2010) 349–353, https://doi.org/10.1126/science.1195552.

[103] S. Fischer, A. Exner, K. Zielske, J. Perlich, S. Deloudi, W. Steurer, P. Lindner, S. Förster, Colloidal quasicrystals with 12-fold and 18-fold diffraction symmetry, Proc. Natl. Acad. Sci. U. S. A. 108 (2011) 1810–1814, https://doi.org/10.1073/pnas.1008695108.

[104] J. Zhang, F.S. Bates, Dodecagonal quasicrystalline morphology in a poly(styrene-b-isoprene-b-styrene-b-ethylene oxide) tetrablock terpolymer, J. Am. Chem. Soc. 134 (2012) 7636–7639, https://doi.org/10.1021/ja301770v.

[105] T.M. Gillard, S. Lee, F.S. Bates, Dodecagonal quasicrystalline order in a diblock copolymer melt, Proc. Natl. Acad. Sci. U.S.A. 113 (2016) 5167–5172, https://doi.org/10.1073/pnas.1601692113.

[106] K. Kim, M.W. Schulze, A. Arora, R.M. Lewis, M.A. Hillmyer, K.D. Dorfman, F. S. Bates, Thermal processing of diblock copolymer melts mimics metallurgy, Science 356 (2017) 520–523, https://doi.org/10.1126/science.aam7212.

[107] Y. Sun, R. Tan, Z. Ma, Z. Gan, G. Li, D. Zhou, Y. Shao, W.B. Zhang, R. Zhang, X. H. Dong, Discrete block copolymers with diverse architectures: resolving complex spherical phases with one monomer resolution, ACS Cent. Sci. 6 (2020) 1386–1393, https://doi.org/10.1021/acscentsci.0c00798.

[108] M. Peterca, V. Percec, Recasting metal alloy phases with block copolymers, Science 330 (2010) 330–334, https://doi.org/10.1126/science.1196698.

[109] D.V. Perroni, M.K. Mahanthappa, Inverse *Pm3n*, cubic micellar lyotropic phases from zwitterionic triazolium gemini surfactants, Soft Matter 9 (2013) 7919–7922, https://doi.org/10.1039/C3SM51238J.

[110] S.A. Kim, K.J. Jeong, A. Yethiraj, M.K. Mahanthappa, Low-symmetry sphere packings of simple surfactant micelles induced by ionic sphericity, Proc. Natl. Acad. Sci. U.S.A. 114 (2017) 4072–4077, https://doi.org/10.1073/pnas.1701608114.

[111] C.M. Baez-Cotto, M.K. Mahanthappa, Micellar mimicry of intermetallic C14 and C15 laves phases by aqueous lyotropic self-assembly, ACS Nano 12 (2018) 3226–3234, https://doi.org/10.1021/acsnano.7b07475.

[112] A. Jayaraman, D.Y. Zhang, B.L. Dewing, M.K. Mahanthappa, Path-dependent preparation of complex micelle packings of a hydrated diblock oligomer, ACS Cent. Sci. 5 (2019) 619–628, https://doi.org/10.1021/acscentsci.8b00903.

[113] M. Huang, C.H. Hsu, J. Wang, S. Mei, X. Dong, Y. Li, M. Li, H. Liu, W. Zhang, T. Aida, W.-.B. Zhang, K. Yue, S.Z.D. Cheng, Selective assemblies of giant tetrahedra via precisely controlled positional interactions, Science 348 (2015) 424–428, https://doi.org/10.1126/science.aaa2421.

[114] K. Yue, M. Huang, R.L. Marson, J. He, J. Huang, Z. Zhou, J. Wang, C. Liu, X. Yan, K. Wu, Z. Guo, H. Liu, W. Zhang, P. Ni, C. Wesdemiotis, W.B. Zhang, S.C. Glotzer, S.Z.D. Cheng, Geometry induced sequence of nanoscale Frank–Kasper and quasicrystal mesophases in giant surfactants, Proc. Natl. Acad. Sci. U.S.A. 113 (2016) 14195–14200, https://doi.org/10.1073/pnas.1609422113.

[115] X. Feng, R. Zhang, Y. Li, Y. Hong, D. Guo, K. Lang, K.Y. Wu, M. Huang, J. Mao, C. Wesdemiotis, Y. Nishiyama, W. Zhang, W. Zhang, T. Miyoshi, T. Li, S.Z. D. Cheng, Hierarchical self-organization of AB_n dendron-like molecules into a supramolecular lattice sequence, ACS Cent. Sci. 3 (2017) 860–867, https://doi.org/10.1021/acscentsci.7b00188.

[116] X. Feng, R. Zhang, Y. Li, Y. Hong, D. Guo, K. Lang, K.Y. Wu, M. Huang, J. Mao, C. Wesdemiotis, Y. Nishiyama, W. Zhang, W. Zhang, T. Miyoshi, T. Li, S.Z. D. Cheng, Hierarchical self-organization of AB_n dendron-like molecules into a supramolecular lattice sequence, ACS Cent. Sci. 3 (2017) 860–867, https://doi.org/10.1021/acscentsci.7b00188.

[117] Z. Su, C.H. Hsu, Z. Gong, X. Feng, J. Huang, R. Zhang, Y. Wang, J. Mao, C. Wesdemiotis, T. Li, S. Seifert, W. Zhang, T. Aida, M. Huang, S.Z.D. Cheng, Identification of a Frank–Kasper Z phase from shape amphiphile self-assembly, Nat. Chem. 11 (2019) 899–905, https://doi.org/10.1038/s41557-019-0330-x.

[118] Y. Liu, T. Liu, X. Yan, Q.Y. Guo, J. Wang, R. Zhang, S. Zhang, Z. Su, J. Huang, G. X. Liu, W. Zhang, W. Zhang, T. Aida, K. Yue, M. Huang, S.Z.D. Cheng, Mesoatom alloys *via* self-sorting approach of giant molecules blends, Giant 4 (2020), 100031, https://doi.org/10.1016/j.giant.2020.100031.

[119] Y. Liu, T. Liu, X.Y. Yan, Q.Y. Guo, H. Lei, Z. Huang, R. Zhang, Y. Wang, J. Wang, F. Liu, F.G. Bian, E.W. Meijer, T. Aida, M. Huang, S.Z.D. Cheng, Expanding quasiperiodicity in soft matter: supramolecular decagonal quasicrystals by binary giant molecule blends, Proc. Natl. Acad. Sci. U.S.A. 119 (2022), https://doi.org/10.1073/pnas.2115304119.

[120] G.C. Shearman, A.I.I. Tyler, N.J. Brooks, R.H. Templer, O. Ces, R.V. Law, J. M. Seddon, Ordered micellar and inverse micellar lyotropic phases, Liq. Cryst. 37 (2010) 679–694, https://doi.org/10.1080/02678292.2010.484917.

[121] D.V. Talapin, E.V. Shevchenko, M.I. Bodnarchuk, X. Ye, J. Chen, C.B. Murray, Quasicrystalline order in self-assembled binary nanoparticle superlattices, Nature 461 (2009) 964–967, https://doi.org/10.1038/nature08439.

[122] X. Ye, J. Chen, M.E. Irrgang, M. Engel, A. Dong, S.C. Glotzer, C.B. Murray, Quasicrystalline nanocrystal superlattice with partial matching rules, Nat. Mater. 16 (2016) 214–219, https://doi.org/10.1038/nmat4759.

[123] M. Girard, S. Wang, J.S. Du, A. Das, Z. Huang, V.P. Dravid, B. Lee, C.A. Mirkin, M. O. de la Cruz, Particle analogs of electrons in colloidal crystals, Science 364 (2019) 1174–1178, https://doi.org/10.1126/science.aaw8237.

[124] K.K. Lachmayr, C.M. Wentz, L.R. Sita, An exceptionally stable and scalable sugar–polyolefin Frank–Kasper A15 phase, Angew. Chem. Int. Ed. 59 (2020) 1521–1526, https://doi.org/10.1002/anie.201912648.

[125] K.K. Lachmayr, L.R. Sita, Small-molecule modulation of soft-matter Frank-Kasper phases: a method for adding function to form, Angew. Chem. Int. Ed. 59 (2020) 3563–3567, https://doi.org/10.1002/anie.201915416.